

***Determination of He and D
permeability of neutron-
irradiated SiC tubes to
examine the potential for
release due to micro-
cracking***

**Nuclear Technology
Research and Development**

**Approved for public release.
Distribution is unlimited.**

*Prepared for
U.S. Department of Energy
Advanced Fuels Campaign
Xunxiang Hu, Takaaki Koyanagi,
Gyanender P. Singh, Yutai Katoh
Oak Ridge National Laboratory
July 21, 2017
ORNL-TM-2017/362*



DISCLAIMER

This information was prepared as an account of work sponsored by an agency of the U.S. Government. Neither the U.S. Government nor any agency thereof, nor any of their employees, makes any warranty, expressed or implied, or assumes any legal liability or responsibility for the accuracy, completeness, or usefulness, of any information, apparatus, product, or process disclosed, or represents that its use would not infringe privately owned rights. References herein to any specific commercial product, process, or service by trade name, trade mark, manufacturer, or otherwise, does not necessarily constitute or imply its endorsement, recommendation, or favoring by the U.S. Government or any agency thereof. The views and opinions of authors expressed herein do not necessarily state or reflect those of the U.S. Government or any agency thereof.

SUMMARY

Driven by the need to enlarge the safety margins of light water reactors in both design-basis and beyond-design-basis accident scenarios, the research and development of accident-tolerant fuel (ATF) has become an importance topic in the nuclear engineering and materials community. Continuous SiC fiber-reinforced SiC matrix ceramic composites are under consideration as a replacement for traditional zirconium alloy cladding owing to their high-temperature stability, chemical inertness, and exceptional irradiation resistance. Among the key technical feasibility issues, potential failure of the fission product containment due to probabilistic penetrating cracking has been identified as one of the two most critical feasibility issues, together with the radiolysis-assisted hydrothermal corrosion of SiC. The experimental capability to evaluate the hermeticity of SiC-based claddings is an urgent need.

In this report, we present the development of a comprehensive permeation testing station established in the Low Activation Materials Development and Analysis laboratory at Oak Ridge National Laboratory. Preliminary results for the hermeticity evaluation of un-irradiated monolithic SiC tubes, uncoated and coated SiC/SiC composite tubes, and neutron-irradiated monolithic SiC tubes at room temperature are exhibited. The results indicate that this new permeation testing station is capable of evaluating the hermeticity of SiC-based tubes by determining the helium and deuterium permeation flux as a function of gas pressure at a high resolution of 8.07×10^{-12} atm-cc/s for helium and 2.83×10^{-12} atm-cc/s for deuterium, respectively. The detection limit of this system is sufficient to evaluate the maximum allowable helium leakage rate of lab-scale tubular samples, which is linearly extrapolated from the evaluation standard used for a commercial as-manufactured light water reactor fuel rod at room temperature.

The un-irradiated monolithic SiC tube is hermetic, as is manifested by the un-detectable deuterium permeation flux at various feeding gas pressures. A large helium leakage rate was detected for the uncoated SiC/SiC composite tube exposed to atmosphere, indicating it is inherently not hermetic. The hermeticity of coated SiC/SiC composite tubes is strongly dependent on the coating materials and the preparation of the substrate SiC/SiC composite samples. To simulate the practical application environment, monolithic CVD SiC tubes were exposed to neutron irradiation at the High Flux Isotope Reactor under high heat flux from the internal surface to the external surface. Although finite element analysis and resonant ultrasound spectroscopy measurement indicated that the combined neutron irradiation and high heat flux gave rise to a high probability of cracking within the sample, the hermeticity evaluation of the tested sample still exhibited gas tightness, emphasizing that SiC cracking is inherently a statistical phenomenon.

The developed permeation testing station is capable of measuring the gas permeation flux in the range of interest with full confidence based on the presented results. It is considered a critical pre-/post-irradiation examination technique to characterize SiC-based cladding materials in as-received and irradiated states to aid the research and development of ATF.

**Determination of He and D permeability of neutron-irradiated SiC tubes to examine the potential
for release due to micro-cracking**

iv

July 21, 2017

CONTENTS

SUMMARY	iii
ACRONYMS	viii
1. INTRODUCTION	1
2. PERMEATION TESTING STATION	3
2.1 DESIGN OF THE PERMEATION TESTING STATION	3
2.2 PERMEATING GAS DETECTION	6
2.3 SAMPLE FIXTURES.....	9
3. HERMETICITY EVALUATION OF AS-RECEIVED, COATED AND NEUTRON-IRRADIATED SiC-BASED TUBES.....	10
3.1 SYSTEM BACKGROUND	10
3.2 GAS PERMEATION THROUGH AS-FABRICATED SiC/SiC COMPOSITE TUBES.....	12
3.3 HERMETICITY EVALUATION OF COATED SiC/SiC COMPOSITE TUBES	15
3.4 HERMETICITY EVALUATION OF NEUTRON-IRRADIATED CVD SiC TUBES UNDER HIGH HEAT FLUX FROM INTERNAL SURFACE TO EXTERNAL SURFACE.....	21
3.4.1 NEUTRON IRRADIATION OF CVD SiC UNDER HIGH HEAT FLUX.....	21
3.4.2 BRIEF INTRODUCTION OF POST-IRRADIATION EXAMINATION AND MODELING OF NEUTRON-IRRADIATED CVD SiC TUBE	21
3.4.3 HERMETICITY EVALUATION OF NEUTRON-IRRADIATED CVD SiC SAMPLE..	27
4. CONCLUSION AND FUTURE WORK	28
5. ACKNOWLEDGEMENT	30
6. REFERENCES	30
APPENDIX A PERMEATION TESTING RESULTS FOR ALL FIVE COATED SAMPLES THAT ARE HERMETIC IN ATMOSPHERE.....	32

FIGURES

Figure 1. (a) Schematic layout and (b) picture of the permeation testing station.....	4
Figure 2. Illustration of the dynamic process in the measurement chamber.	6
Figure 3. (a) Engineering plot of the standard gas leak apparatus. (b) Picture of the calibration system of the permeation testing station.....	7
Figure 4. Mass spectrometer signals during the calibration process.	8
Figure 5. (a) ConFlat flange used to hold samples; (b) picture of sample assembly; and (c) sample assembly located in the tube furnace.....	10

Figure 6. Deuterium permeation flux through the CVD SiC at room temperature as a function of gas pressure. The signals for the major gas elements in the background were also given in the same plot	11
Figure 7. As-fabricated SiC/SiC composite tube without any surface treatment	12
Figure 8. As fabricated SiC/SiC tube N3 (10) with inner and outer surfaces coated with CVD SiC.....	13
Figure 9. (a) Helium and (b) deuterium permeation flux through N3(10) as a function of applied gas pressure.....	14
Figure 10. Helium and deuterium permeation flux through N3(10) as a function of feeding gas pressure. The dashed line indicates the correlation between gas pressure and gas permeability in the materials.	15
Figure 11. Mass spectrometer signals of gas elements captured in the downstream section of the permeation testing station of coated (a) GA-TGI-D6 and (b) N1N3(9) samples as a function of deuterium pressure. The major remaining gas elements in the system are also shown.	17
Figure 12. Images of coated (a) GA-TGI-D7, (b) N1N3(7), (c) GA-TGI-D6, (d) N1N3(9), (e) N1N3(10), (f) GA-TGI-D2, (g) N1N3(13), and (h) GA-TGI-D3.....	19
Figure 13. Helium and deuterium permeation flux through the coated N1N3(9) and N1N3(13) tubes as a function of feeding gas pressure.....	20
Figure 14. Temperature distribution across the CVD SiC tube during irradiation under a radial high heat flux.....	22
Figure 15. (a) Scanning areas during the Raman spectroscopy measurements; (b) Correlation between the longitudinal optical phonon line shift and the irradiation temperature.	22
Figure 16. (a) Axial stress and (b) hoop stress distribution in the neutron-irradiated CVD SiC tube. Positive stress indicated tension and negative stress indicates compression (Unit: Pa).....	23
Figure 17. Frequency spectra of unirradiated and irradiated CVD SiC tubes.	24
Figure 18. Numerically obtained vibration modes for a CVD SiC tube sample.	25
Figure 19. Modulus change as a function of swelling for the neutron-irradiated CVD SiC specimen	26
Figure 20. Cross section images of un-irradiated and neutron-irradiated CVD SiC tubular specimens....	27
Figure 21. (a) Helium and (b) deuterium permeation flux through neutron-irradiated CVD SiC as a function of applied gas pressure.	28

TABLES

Table 1. Major technical specifications of the permeation testing station.....	6
Table 2. Calibration results by using standard gas leaks	8
Table 3. Hermeticity evaluation of coated SiC/SiC tubes at room temperature.....	16
Table 4. Elastic modulus changes for two CVD SiC tubes before and after neutron irradiation.	24

**Determination of He and D permeability of neutron-irradiated SiC tubes to examine the potential
for release due to micro-cracking**

July 21, 2017

vii

ACRONYMS

ATF – Accident Tolerant Fuel

CF – ConFlat

CVD – Chemical Vapor Deposited

CVI – Chemical Vapor Infiltration

DOE – Department of Energy

FEA – Finite Element Analysis

HFIR – High Flux Isotope Reactor

LAMDA – Low Activation Materials Development and Analysis

LWR – Light Water Reactor

ORNL – Oak Ridge National Laboratory

PVD – Physical Vapor Deposition

RT – Room Temperature

RUS – Resonant Ultrasound Spectroscopy

SiC – Silicon Carbide

SiC/SiC – SiC fiber reinforced SiC matrix ceramic composites

SS – Stainless Steel

TRISO – Tristructural-Isotropic

UHP – Ultra-High Purity

UHV – Ultra-High Vacuum

VCR – Vacuum Coupling Radiation

DETERMINATION OF HE AND D PERMEABILITY OF NEUTRON-IRRADIATED SiC TUBES TO EXAMINE THE POTENTIAL FOR RELEASE DUE TO MICRO-CRACKING

1. INTRODUCTION

Since the 2012 Japan Fukushima nuclear disaster, a new concept of nuclear fuel, accident tolerant fuel (ATF), has been emerging in the nuclear engineering and materials community [1] [2] [3]. ATF aims to enlarge the safety margins of the current light water reactors (LWRs) under design basis or beyond design basis accident scenarios. In the current nuclear reactor fleet, zirconium alloys are the primary fuel cladding and core structural materials. However, zirconium alloys are vulnerable to catastrophic failure in severe accidents [4], which is attributed primarily to the rapid oxidation kinetics of zirconium in a high temperature steam environment [5]. As the first safety boundary of nuclear reactors, alternative fuel cladding materials with enhanced oxidation resistance have been perceived to improve the accident tolerance of nuclear fuels. FeCrAl alloys [3] and silicon carbide (SiC) fiber reinforced SiC matrix (SiC/SiC) composites [6] are the two leading candidate ATF cladding materials. Oxidation rates for these materials are several orders of magnitude lower than that of zirconium alloys [4]. The reduced oxidation rates in these materials lead to reduced heating and hydrogen generation in the core as a result of this exothermic reaction, which ultimately leads to a slower rate of temperature rise in the reactor core.

As one of the leading ATF cladding materials, SiC/SiC composites have been thoroughly investigated with respect to technical feasibility for fuel cladding applications at Oak Ridge National Laboratory (ORNL) under the Advanced Fuels Campaign. Actually, SiC is not new to the nuclear community as it has been widely applied or considered in nuclear systems as a fuel and structural material since the 1960s, given its high-temperature stability, chemical inertness, and exceptional irradiation resistance [7]. For example, chemical vapor-deposited (CVD) SiC has been considered as a pressure vessel material for the tristructural-isotropic (TRISO) fuel particles used in high temperature gas-cooled reactors [8]. The use of SiC/SiC composites as primary structural materials has also been proposed in fusion reactors [9]. Now SiC is envisioned as a potential cladding material for LWRs to enhance their accident tolerance. Although high-purity SiC has numerous merits in comparison with zirconium alloys for service in reactors, monolithic SiC alone has low fracture toughness. That makes it inappropriate for nuclear fuel cladding applications because a fuel cladding needs to be robust, as it is considered the first safety boundary for retaining fission products, especially under transient or off-normal conditions. The proposed solution is to employ an engineered composite structure to address the brittle behavior, using strong SiC fibers reinforcing an SiC matrix to form an SiC/SiC composite [10].

Nuclear-grade SiC/SiC composites are typically fabricated using chemical vapor infiltration (CVI), which employs a stoichiometric and crystalline beta-phase SiC matrix, near-stoichiometric crystalline SiC fibers, and a monolayer carbon interphase or multilayer C/SiC interphase. CVI is considered a low-temperature processing method for the fabrication of SiC matrix composites,

with the benefits of minimal process-induced damage to the fibers and reduced residual thermal stress [10]. However, CVI composites inherently consist of fabric layup architectures made up of small, elongated inter-fiber pores with more macroscopic inter-bundle pores. The porosities of as-fabricated CVI SiC/SiC composites are usually in the range of 15~20%, and it is challenging to reach very low porosity levels. Therefore, a CVD SiC coating is typically applied inside and/or outside the cladding, depending on the particular material design, to provide the required gas tightness. Although SiC/SiC composites undergo pseudo-ductile fracture rather than brittle failure, micro-cracking may occur during the process or under the expected in-pile stress state [11], which can lead to a loss of hermeticity. Therefore, it is important to understand the relationship between micro-cracking behavior and the hermeticity of these SiC/SiC composite tubes. Another challenge to the feasibility of SiC/SiC composite cladding is the hydrothermal corrosion of SiC in a reactor coolant environment [12]. A thermodynamic driving force always exists to cause the silicon in SiC to undergo oxidation and produce silica, which readily dissolves in water. Therefore, a loss of cladding thickness is expected, imposing challenges to safety. As a consequence, the composite alone may not be sufficient to contain fission gases within the fuel cladding. Therefore, an impermeable fission gas barrier with improved hydrothermal corrosion resistance on the surface of the composite tubes may be necessary. Metallic coatings could be a solution [13]. In addition to these two most critical feasibility issues, other outstanding challenges to the use of this class of structural materials as a fuel cladding in commercial fission reactors include defining a path toward a significant reduction in the fabrication costs, improving joining techniques, and investigating fuel pellet-cladding mechanical interactions [1] [6].

A SiC/SiC composite cladding must meet a range of material property and performance requirements to fulfill the “drop-in replacement” objective of the Department of Energy (DOE) related to the development of ATF cladding [1]. The implementation of SiC/SiC composite cladding in LWRs requires a thorough understanding and characterization of the composite cladding before and after neutron irradiation, including the mechanical properties, hermeticity, and performance of the environmental barrier coating. In addition to the enhanced accident tolerance resulting from the use of the continuous fiber SiC/SiC composite cladding, a primary function of the cladding itself is to maintain an impermeable barrier to prevent fission gas release from the fuel into the reactor primary coolants. A criterion of SiC/SiC composite cladding failure is the loss of gas tightness. Any increase in the extent of fission gas release from the fuel will be directly proportional to an increase in the radioactivity in the primary coolant and the fission gas (e.g., tritium) release to the environment. Moreover, helium is used as the heat conduction medium between the fuel and the cladding. A loss of hermeticity would lead to the release of helium. As a consequence, the heat produced in the fuel could not be removed efficiently and the probability of fuel failure would increase. The maximum allowable leakage rate for an as-manufactured LWR fuel rod is 1.0×10^{-6} atm-cc/sec when pressurized with helium to 1.7 MPa at room temperature (RT) [14]. The gas tightness of the as-fabricated and coated SiC/SiC composite tubes needs to be tested to determine whether this criterion is met for their application in LWRs.

Gas permeability data for SiC and SiC/SiC composites in tubular configurations is very limited, especially for samples subjected to neutron irradiation. It is well known that hydrogen permeability in monolithic SiC is extremely low, ~ ten orders of magnitude lower than that in stainless steels. Therefore, SiC is usually used as barrier for hydrogen isotopes [15] [16]. Hydrogen permeability in SiC is strongly dependent on the manufacturing methods and the quality of the samples

produced. CVD beta SiC has shown the lowest hydrogen permeability [16]. Hino et al. measured the helium gas permeability of planar SiC/SiC composite samples. The measured helium permeability had a wide range from 10^{-11} to 10^{-5} m²/s, roughly dependent on the pore structure of the SiC fiber bundle and SiC matrix layers [17] [18]. Since SiC/SiC composites were perceived as a promising ATF cladding material, a research group at General Atomics investigated the gas tightness of tubular SiC and SiC/SiC composite samples using a mobile helium leak detector [13] [19] to characterize the quality of the as-fabricated SiC-based claddings.

However, an experimental capability to evaluate the hermeticity of neutron-irradiated SiC-based cladding has not been available up to now. This report summarizes our efforts to develop an experimental capability for measuring the gas permeation flux through pristine and coated SiC/SiC composite tubes under un-irradiated and irradiated conditions as a function of gas pressure at elevated temperatures. Section 2 is a detailed introduction to the comprehensive permeation testing station established in the Low Activation Materials Development and Analysis (LAMDA) laboratory at ORNL. Section 3 presents measurements of the helium and deuterium permeation flux through various SiC-based tubes. Section 4 summarizes the results presented in this report and lays out the future work.

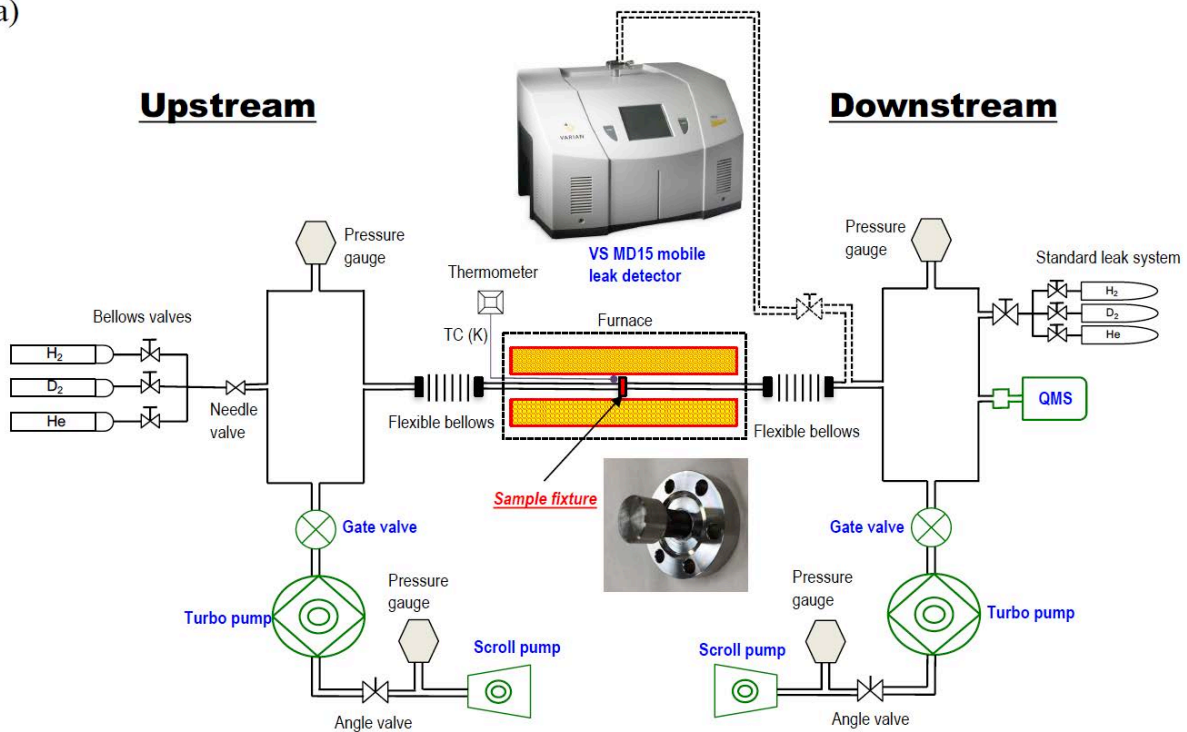
2. PERMEATION TESTING STATION

Gas permeation flux through SiC-based claddings is considered an important indicator to evaluate the hermeticity of the studied materials. The term of “permeation testing” encompasses the gas leakage measurements due to physical openings through the walls of the materials (e.g, penetrating cracking) and the actual gas permeability (an intrinsic physical property, equal to the product of diffusivity and solubility) in a material. The testing methods for both parameters are the same. A comprehensive permeation testing station has been constructed in the LADMA lab at ORNL that is capable of measuring extremely low helium, deuterium and hydrogen permeation flux through the studied materials as a function of the feeding gas pressure at elevated temperature.

2.1 Design of the Permeation Testing Station

As mentioned in the Introduction, the maximum allowable helium leakage rate for an as-manufactured LWR fuel rod is 1.0×10^{-6} atm-cc/sec when pressurized with helium to 1.7 MPa at room temperature. Assuming the gas leakage rate through a tubular SiC-based sample is proportional to the gas pressure and sample surface area, the corresponding maximum allowable helium leak rates for lab-scale SiC-based tubes can be extrapolated. Therefore, the standard for a tubular sample with a diameter of 8.5 mm and a length of 16.2 mm, the most commonly used sample configuration in the current study, would be 2.2×10^{-10} atm cc/sec, if a test pressure difference of 1 atm was assumed. The detection limit of the permeation testing station should be lower than this value. Therefore, the need to measure the low fluxes expected for SiC-based tubes was a major consideration in the design of the high-temperature permeation testing station. Ultra-high vacuum (UHV) is necessary to enable the clean background required for the extremely low detection limit.

(a)



(b)

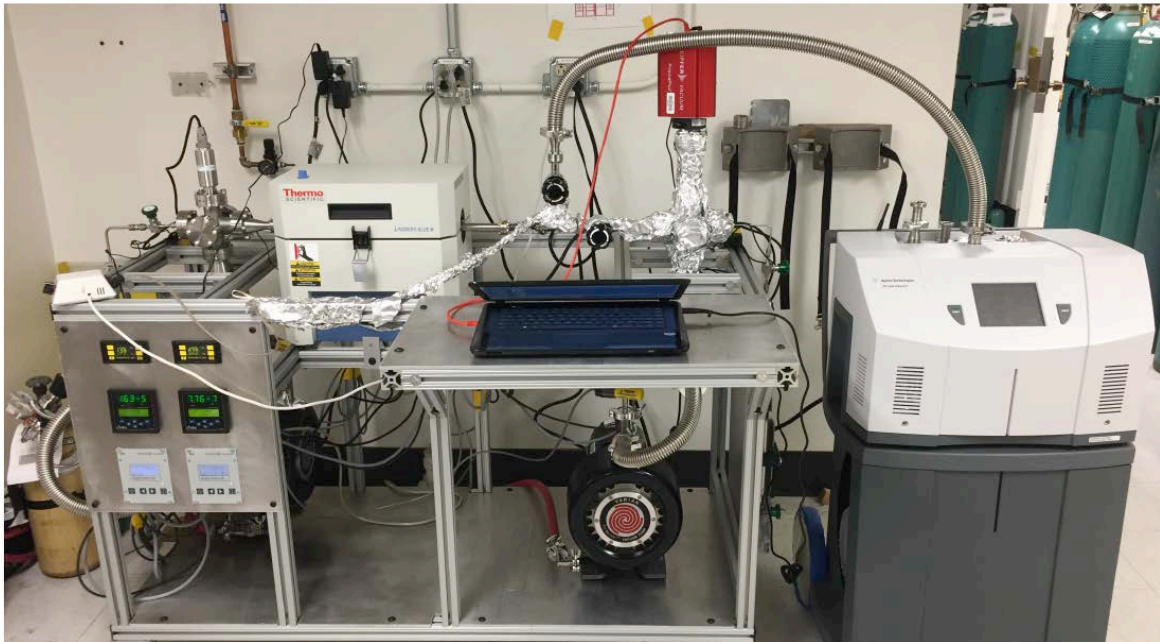


Figure 1. (a) Schematic layout and (b) picture of the permeation testing station.

A UHV device consisting of a high-pressure chamber and a low-pressure chamber, corresponding to the upstream side and downstream side, respectively, was constructed. Figure 1 shows a schematic illustration and picture of the permeation testing system. The system was constructed with commercial stainless steel vacuum components and all-metal valves. It consists of two major parts: the upstream section providing the testing gas at a desired pressure and the downstream section measuring the permeating gas. These two sections are connected through a sample fixture in which the sample of interest is used as the vacuum boundary. The sample fixture is placed in a tube furnace (an electric resistance furnace), with a maximum temperature of 1000°C. Three types of feeding gases could be used in this system—He, H₂, and D₂.

The upstream chamber is equipped with a Pfeiffer HiPace 80 turbo-drag-pump (71 L/s) in which the pre-vacuum is obtained by the deployment of a Varian TriScroll 600 oil-free dry scroll vacuum pump to aid in outgassing of the system. The UHV level of the upstream chamber is $\sim 1 \times 10^{-7}$ torr. When this vacuum level is reached, the manual gate valve connecting the vacuum chamber and the turbo pump is closed. Then ultra-high purity (UHP) working gas is introduced to the upstream vacuum chamber. The testing gas was provided from three UHP He, D₂, and H₂ gas cylinders. Among these gases, helium is the one most commonly used to look for the location of a vacuum leak because of its high mobility. Considering that a large amount of tritium could be produced in nuclear fuels through ternary nuclear fissions, hydrogen isotopes were also included as testing gases. The testing gas, controlled by a needle valve, is introduced into the upstream vacuum chamber at the desired pressure. The pressure of the gas is measured by an MKS 909AR digital and analog hot cathode vacuum transducer. The pressure of the feeding gas ranges from 1×10^{-7} torr to 900 torr. A constant gas pressure is expected to be attained within several seconds; this quick control reduces the measurement error of the lag time and then the effective diffusivity. Flexible bellows are used to connect the vacuum chamber and the sample fixture, which allows flexibility in exchanging the sample fixtures for various measurements.

In the downstream section of the system, the same vacuum level of $\sim 1 \times 10^{-7}$ torr is achieved using a pumping system that is identical to the upstream section. Metal valves are used where possible to further limit residual gases in the system. When pressurized feeding gas is applied in the upstream section, the permeating gas through the sample is captured by using a quadrupole mass spectrometer as a function of time. The Pfeiffer PrismaPlus QMG 220 compact mass spectrometer covers a mass range from 1 to 100 amu. In addition, a separate Agilent VS MD15 mobile helium mass spectrometer leak detector with a minimum detectable leak rate of 1×10^{-12} atm-cc/sec is included. This mobile helium leak detector provides a quick evaluation of the hermeticity of the studied samples exposed to atmosphere and the ability to measure the large helium leakage rates when significant cracking occurs in the sample. The major technical specifications of this system are listed in Table 1.

Table 1. Major technical specifications of the permeation testing station

		Parameter
	Sample type	Un-irradiated or neutron-irradiated
	Specimen geometry	Planar or tubular
Size	Planar specimen	6 mm or 11 mm
	Tubular specimen	8.5~10 mm in diameter, flexible length
Testing temperature	Planar specimen	Room temperature ~ 800°C
	Tubular specimen	Room temperature ~ 350°C
	Sample seal methods	Mechanical seal + high temperature epoxy
	Testing gas	He, H ₂ , and D ₂
	Ultimate vacuum level	1×10^{-7} torr
	Pressure difference between upstream and downstream during testing	1×10^{-7} torr ~ 900 torr
	Detection limit of the mobile He leak	1×10^{-12} atm-cc/sec
	Detection limit of the quadrupole mass spectrometer	8.07×10^{-12} atm-cc/sec for helium 2.83×10^{-12} atm-cc/sec for deuterium

2.2 Permeating Gas Detection

The detection of permeating gas through the sample, the vacuum boundary separating the upstream and downstream vacuum chamber, is carried out using a PrismaPlus QMG 220 compact mass spectrometer. A linear correlation exists between the ion current in the mass spectrometer and the gas partial pressure in the downstream vacuum chamber:

$$I(A) \propto P \text{ (torr)} \quad (1)$$

As shown in Figure 2, the change rate of gas amount in the measurement chamber can be expressed as

$$R_{change} = R_{permeation} - R_{pumping} \quad (2)$$

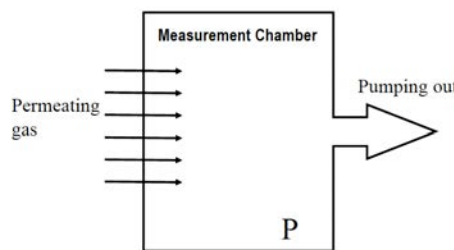


Figure 2. Illustration of the dynamic process in the measurement chamber.

The change rate of the gas amount in the measurement chamber with constant volume and temperature can be written as

$$R_{change} = \frac{V}{k_B T} \frac{dP}{dt} \quad (3)$$

The extracting rate of gas from the measurement chamber is

$$R_{pumping} = \frac{V}{k_B T} \frac{P}{\tau} \quad (4)$$

where V is the volume of the system; P is the pressure of the measurement chamber; k_B is the Boltzmann constant; T is the temperature; t is the time; and $\tau = V / S$ is the pumping time constant with S being the pumping speed (volume per unit time) of the measurement chamber.

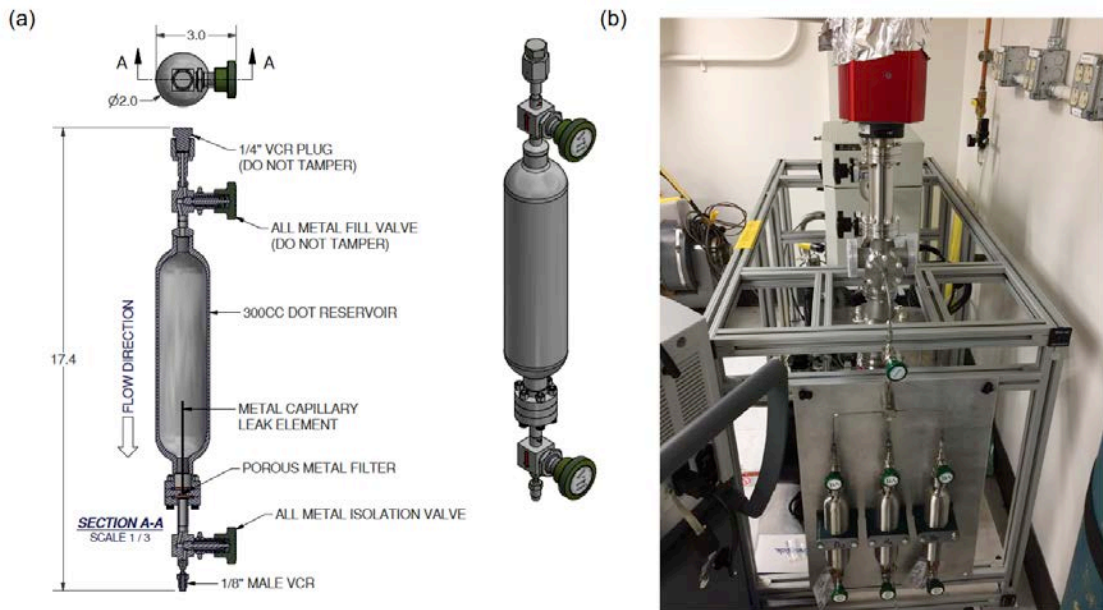


Figure 3. (a) Engineering plot of the standard gas leak apparatus. (b) Picture of the calibration system of the permeation testing station.

Therefore, the desired gas permeation rate through the sample is given by

$$R_{permeation} = \frac{V}{k_B T} \left(\frac{dP}{dt} + \frac{P}{\tau} \right) \quad (5)$$

During the measurement, the measurement chamber is always in an UHV environment and the system pressure stabilizes at $\sim 1 \times 10^{-7}$ torr. Therefore, dP/dt in Eq. (5) is negligible, and the following correlation can be obtained,

$$R_{permeation} \propto P \propto I \quad (6)$$

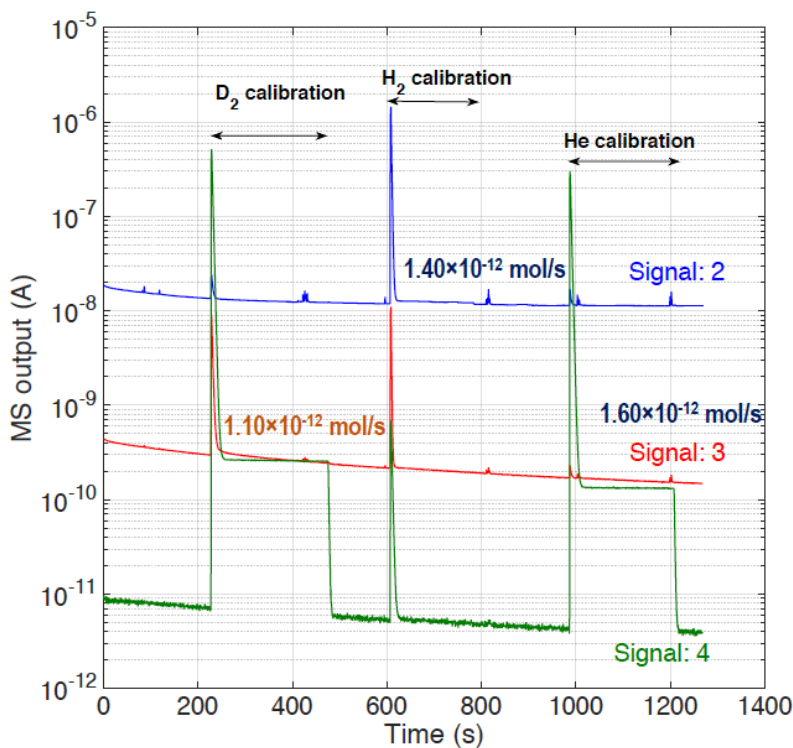


Figure 4. Mass spectrometer signals during the calibration process.

Table 2. Calibration results by using standard gas leaks.

Gas type	Mass-to-charge ratio	Mass spectrometer output (A)	Standard gas leak rate (mol/s)	Converting coefficient (mol/C)
Helium	4	1.33×10^{-10}	1.60×10^{-12}	0.012
Deuterium	4	2.59×10^{-10}	1.10×10^{-12}	0.0042
Hydrogen	2	1.06×10^{-9}	1.40×10^{-12}	0.0013

Therefore, the gas permeation rate is approximately proportional to the gas flux detected by using the mass spectrometer. The detected gas information is given in the form of electrical current (I) with a unit of ampere (A) by the mass spectrometer. A calibration process is required to convert the electrical current to the atomic number of the gas elements of interest. It is recommended that the calibration is performed before each measurement, because the sensitivity of the mass spectrometer may alter as a function of time. In this system, three standard leak apparatus (i.e., He, D₂, and H₂) with known constant gas leakage rates, fabricated by VTI Vacuum Tehcnology, Inc., were used to calibrate the mass spectrometer signals (Figure 3). The constant gas leakage rates of He, D₂ and H₂ standard leaks were 1.60×10^{-12} mol/s, 1.10×10^{-12} mol/s, and 1.40×10^{-12} mol/s, respectively. The calibration was performed by opening the standard gas leak apparatus one by one and recording the mass spectrometer signals. The recorded signals during the calibration process are plotted in Figure 4. The abrupt increase in the signal arose from the release of the

accumulated remaining gas inside the valves. Then the converting coefficient between the mass spectrometer output and the atom flux was obtained by applying the linear relationship of these two parameters. The final calibration results are listed in Table 2.

2.3 Sample Fixtures

The permeability of monolithic SiC is extremely low, and developing a versatile fixture to hold specimens that prevents leakage of helium around the fixture while facilitating the measurement of very small leak rates through the sample was challenging. Sample fixtures were designed and fabricated to hold the SiC-based tubes with two open ends or one open end, as shown in Figure 5a. For a tubular sample with two open ends, one end is inserted into the open slot in the perforated stainless steel (SS) ConFlat (CF) flange while the other is covered with an impermeable SS cap (Figure 5b). For a tubular sample with one open end, only the perforated SS CF flange is needed to hold the sample. The application of epoxy as the primary seal is an attractive option since it can conform to the SiC/SiC composite's rough surface without the need for specialized polishing or machining. The epoxy used here was Crystalbond 590, purchased from Electron Microscopy Sciences. Crystalbond 590 was filed into a fine powder to facilitate its application in the small gaps between the sample and the SS sample fixture. Crystalbond 590 was in a solid state at room temperature. The softening point and flow point were 125°C and 150°C, respectively. The attachment process for the tubular sample with two open ends was as follows: stack Crystalbond 590 powder into the SS cap and place it on a hot surface (~150°C); wait until the powder melts, then insert the SiC-based tube into the liquid medium; remove this sample assembly from the hot surface; wait until the liquid Crystalbond is fully cured at room temperature; repeat the same procedure to attach the other open end to the CF flange bottom part. For attaching a tubular sample with one open end, the process was simpler, since the use of the impermeable SS cap was not needed. Note that the current sample fixture is only applicable to the room temperature testing. Permeation testing at elevated temperature requires the use of high temperature epoxy as primary seal, which is being investigated.

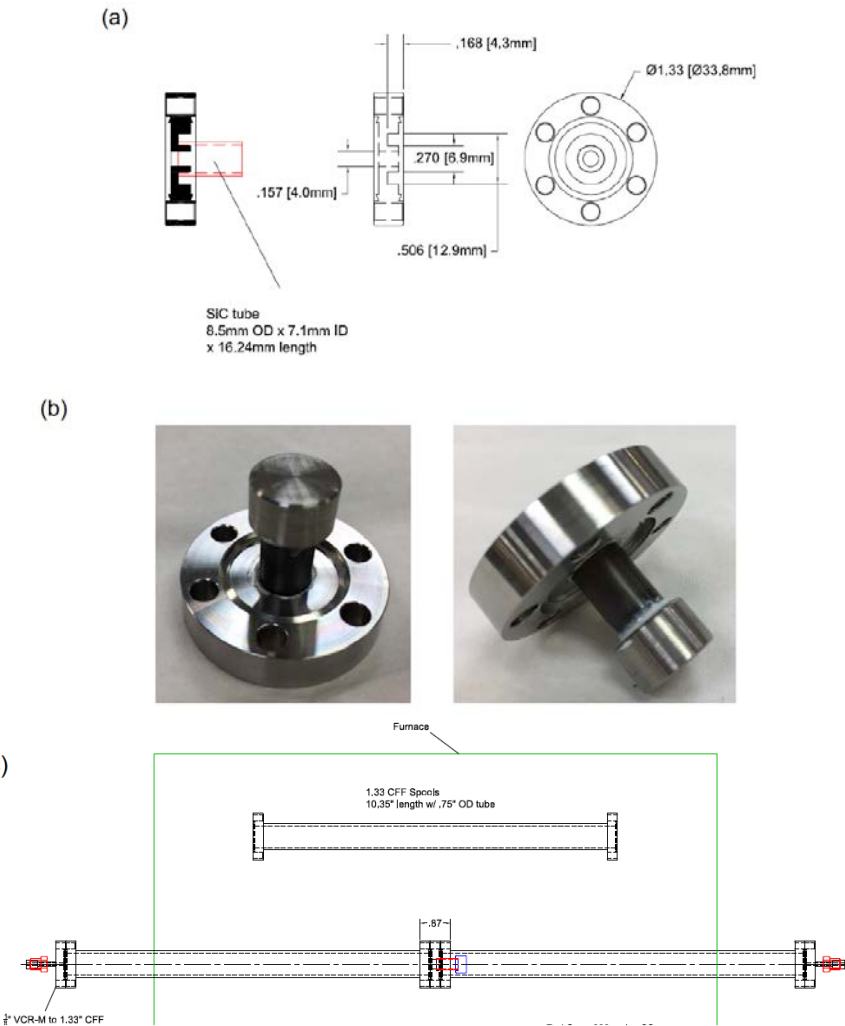


Figure 5. (a) ConFlat flange used to hold samples; (b) picture of sample assembly; and (c) sample assembly located in the tube furnace.

After the sample tube is attached to the sample fixture, it is fixed between two SS tubes with CF flange connections and sealed with copper gaskets. Then the whole sample assembly is inserted into the tube furnace and then connected to the vacuum chambers through vacuum coupling radiation (VCR) fittings, as shown in Figure 5c.

3. HERMETICITY EVALUATION OF AS-RECEIVED, COATED AND NEUTRON-IRRADIATED SiC-BASED TUBES

3.1 System Background

As the primary seal used to attach the sample to the impermeable SS flange, the permeability data for the crystalbond 590 are needed. The epoxy was applied between an impermeable CVD SiC

disk and a perforated SS conflat flange, and the assembly was installed in the permeation testing station. Then pure helium and deuterium at various pressures were applied in the upstream chamber to evaluate the gas tightness of the epoxy at room temperature as a function of gas pressure. The results showed no change in the measured gas permeation flux at various applied pressures for either helium or deuterium working gas; it remained at very low levels: 8.07×10^{-12} atm-cc/s and 2.83×10^{-12} atm-cc/s for helium and deuterium, respectively. These results also set the detection limits of the permeation testing system for these two working gases.

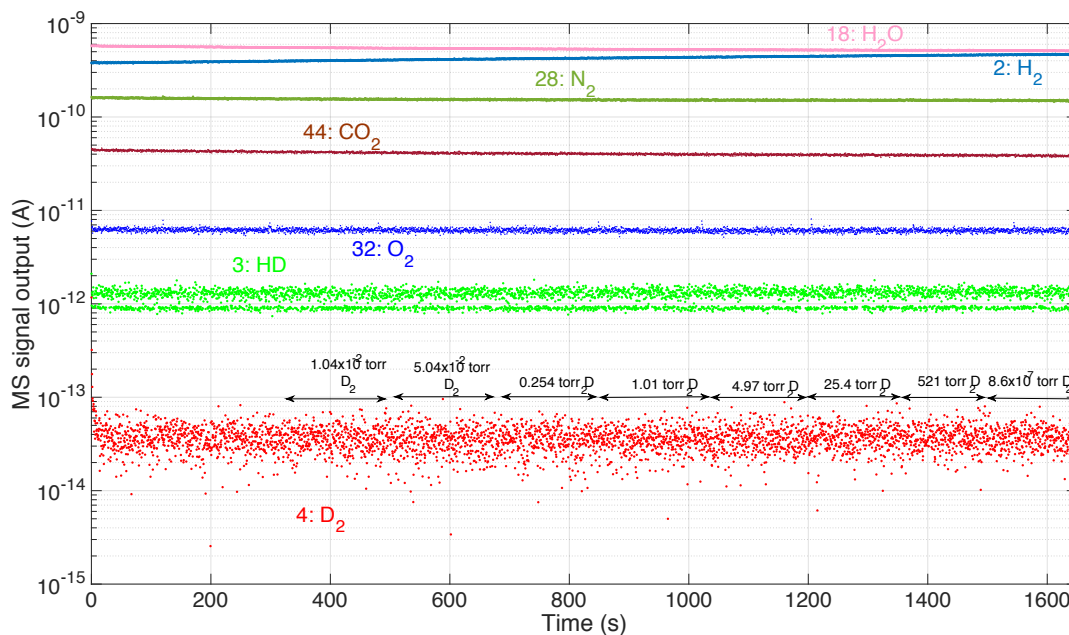


Figure 6. Deuterium permeation flux through the CVD SiC at room temperature as a function of gas pressure. The signals for the major gas elements in the background were also given in the same plot.

It is well known that monolithic CVD SiC is hermetic. Therefore, CVD SiC was also used to validate the developed system. The sample (16 mm in length, 8.5 mm in outside diameter) was first tested using a mobile helium leak detector. The results indicated that the helium leakage rate was less than 1×10^{-12} atm-cc/s when exposed to atmosphere. Figure 6 shows the deuterium permeation flux through the CVD SiC tube when pure deuterium at various pressures were applied in the upstream section of the system. The system was stabilized at each applied gas pressure for 2 mins. The mass spectrometer signal for deuterium remained at a very low level of 3×10^{-14} A (2.83×10^{-12} atm-cc/s), during the entire measuring process, indicating that the CVD SiC tube is hermetic. In addition, the application of pressurized deuterium in the upstream vacuum chamber did not impact the signals of other gaseous elements in the background of the system. Therefore, a clean system background was achieved, giving rise to acceptable detection limits for helium and deuterium.

3.2 Gas Permeation Through As-Fabricated SiC/SiC Composite Tubes

A bare SiC/SiC composite tube without any inner and outer monolithic SiC layer was fabricated by General Atomics INC.. Composite samples were reinforced with stoichiometric SiC fibers (Hi-Nicalon type-S fiber, NGS Advanced Fiber Co.). The tubular sample shown in Figure 7 consists of only SiC-SiC composite without a coating, formed by placing the fiber around a mandrel to define the tube inner diameter. The mandrel was later removed as part of the overall fabrication process. Fiber orientation was varied by adjusting the number of fiber tows used and the angle relative to the tube axis. A pyrolytic carbon interphase coating of ~150nm was deposited via the chemical vapor decomposition of methane or acetylene, and the matrix was then deposited and densified through the chemical vapor infiltration of methyltrichlorosilane to a final relative density of approximately 80%. More details on the fabrication process can be found in Ref. [13]. Because of the intrinsic small, elongated inter-fiber pores and more macroscopic inter-bundle pores (~20% porosity), the as-fabricated SiC/SiC composite tube was not believed to be hermetic.



Figure 7. As-fabricated SiC/SiC composite tube without any surface treatment

The sample assembly shown in Figure 7 was directly connected to the Agilent VS MD15 mobile helium mass spectrometer leak detector. Given the large number of physical openings present in the sample, even a rough vacuum could not be obtained. Therefore, the mobile helium leak detector could not initialize the leak testing, thus verifying the inherent leakage of the as-fabricated SiC/SiC composite tube.

To enhance the gas tightness of the as-fabricated SiC/SiC composite tubes, the inner and outer surfaces of the tubes are usually coated with CVD SiC. As shown in Figure 8, the bottom of a SiC/SiC composite tube (N3(10)) with inner and outer surfaces coated with CVD SiC, was damaged during the surface treatment process. Some local surface areas show the bare SiC fiber bundles, whereas most of the surface areas are in good conditions with a smooth finish.



Figure 8. As fabricated SiC/SiC tube N3 (10) with inner and outer surfaces coated with CVD SiC.

The damaged end was attached to the perforated CF flange by inserting it into the epoxy, avoiding the possible gas permeation through the damaged section. Then the other end was covered with an impermeable SS cap. The sample assembly was connected to the mobile helium leak detector to evaluate its hermeticity when exposed to the atmosphere. The results indicated the helium leakage rate was lower than 1×10^{-12} atm-cc/s, implying the N3(10) sample with a CVD SiC coating was hermetic under this testing condition. However, note that there is only ~5.2 ppm helium by volume in the atmosphere. The hermeticity of the studied SiC/SiC composite tube verified under atmosphere does not guarantee its hermetic performance when it is subjected to a pressurized pure helium environment. In the gas permeation testing station, helium and deuterium at various pressures were applied in the upstream section, respectively, while the gas permeation flux was captured by using the quadrupole mass spectrometer. The system was stabilized at each applied gas pressure for 2 minutes. The results are shown in Figure 9. It is apparent that the helium and deuterium permeation flux through the N3(10) sample was increasing as the pressure of the working gas increased, starting from ~0.01 torr. When the pressure of the applied gas in the upstream section of the system was lower than 1×10^{-3} torr, gas permeation was still undetectable. The increase in the magnitude of the permeation flux following each pressure step decreased when the applied pressure was more than 25 torr in both helium and deuterium applied gas. In the case of the deuterium permeation measurement, isotope exchange was expected when the deuterium permeation flux through the sample increased in the measurement chamber (hydrogen occupied a large fraction in the remaining gases in the background); this led to the production of HD and an increase in the mass spectrometer signal of 3, when the applied deuterium pressure in the upstream section became greater than 25 torr (Figure 9b).

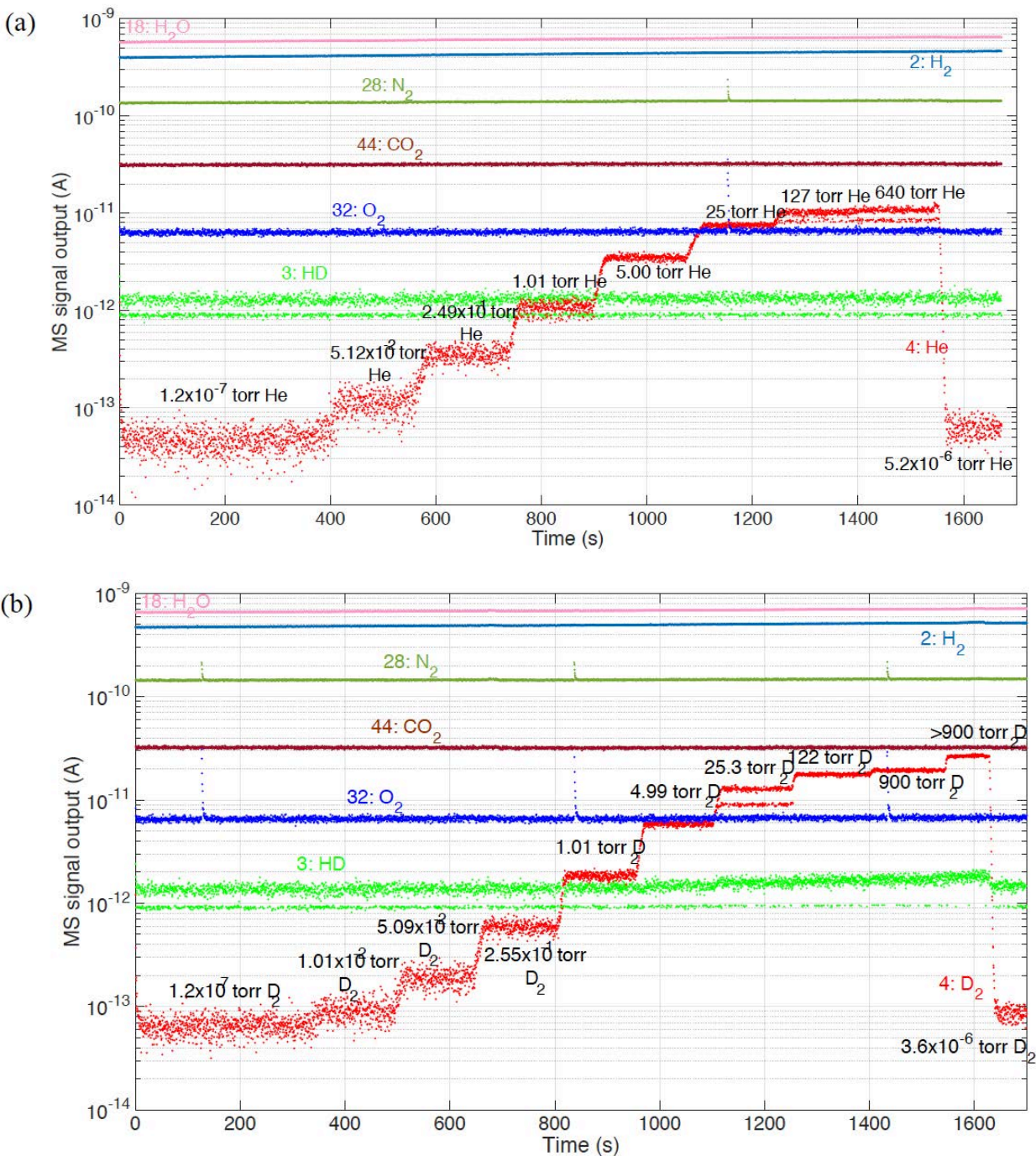


Figure 9. (a) Helium and (b) deuterium permeation flux through N3(10) as a function of applied gas pressure.

To clarify the correlation between the applied gas pressure and the corresponding permeation flux, Figure 10 plots the gas permeation flux as a function of feeding gas pressure. The helium and deuterium permeation rate through the studied material showed similar behavior. When the applied pressure (P) was lower than 25 torr, the permeation flux was proportional to P^n . When P was continuously increasing, the measured permeation flux started to level off and had a trend toward

saturation. The permeation flux of helium was larger than that of deuterium, indicating that helium has higher mobility. It is interesting to compare with the behavior of the gas permeability, the intrinsic physical property of a continuous medium, which is well known to be proportional to $P^{1/2}$, indicated as a dashed line in Figure 10. Apparently, the gas permeation flux through the SiC/SiC composite tube was not diffusion-limited which is completely different from the concept of gas permeability. “Leakage rate” is a more accurate term to describe the gas permeation flux through the penetrating physical openings present within the tube wall.

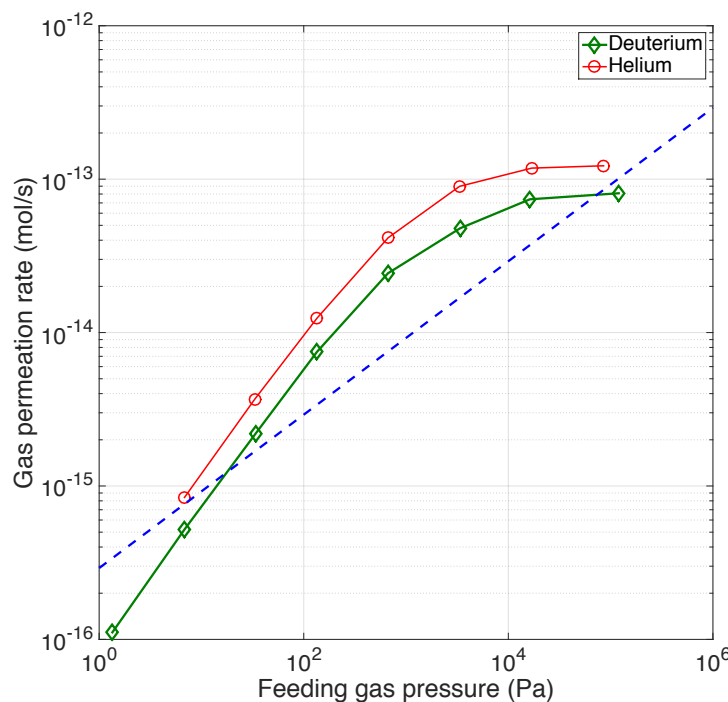


Figure 10. Helium and deuterium permeation flux through N3(10) as a function of feeding gas pressure. The dashed line indicates the correlation between gas pressure and gas permeability in the materials.

3.3 Hermeticity Evaluation of Coated SiC/SiC Composite Tubes

As discussed in the Introduction, hydrothermal corrosion of SiC and the hermeticity of SiC/SiC composite cladding are two critical feasibility issues associated with use of this class of materials as nuclear fuel cladding. Adding a hermetic and hydrothermal corrosion-resistant layer on the SiC/SiC composite tube is one direction of development to prevent or mitigate these two critical issues. Presently chromium-based metallic and ceramic coatings are considered the leading candidates based on the industrial availability of the coating techniques, synergy with research and development of coated zirconium alloy ATF cladding concepts, and the encouraging results from the recent in-pile experiments in the Halden Reactor [20]. The technical hurdles that must be overcome for dual-purpose coated SiC/SiC composite cladding include the need for development of strongly bonded, crack-free coating techniques and the effects of neutron irradiation.

Hermeticity evaluation by using the permeation testing station is one of the key characterization techniques to assess the quality of the developed coating before and after neutron irradiation.

Cathodic arc physical vapor deposition (PVD) technique was carried out to coat three different materials (i.e., TiN, CrN, and Cr) onto the SiC/SiC composite tubes at ORNL. The coating materials were produced from two external vendors: Techmetals Inc., OH (referred to as TM) and Richter Precision, Inc, PA (referred to as RP). A more detailed description of coating on SiC cladding developed at ORNL was published in “*ORNL-TM-2017 – M3FT-17OR020202106 Complete evaluation for the first-generation dual-purpose coating for SiC cladding*”. In the present study, eight coated SiC/SiC tubes were tested by using the established permeation testing system. Initial evaluation of the hermeticity of tested samples was performed using the mass spectrometer helium leak detector to acquire the helium leakage rate through the coated SiC/SiC tubes exposed to atmosphere. Table 3 shows the results for all tested samples.

Table 3. Hermeticity evaluation of coated SiC/SiC tubes at room temperature

Tube materials	Coating materials	Helium leak rate in atmosphere (atm-cc/sec)	Evaluation by using mobile helium leak detector (in atmosphere)	High-pressure testing
GA-TGI-D7	TM-CrN	3.8×10^{-8}	Not hermetic	-
N1N3(7)	TM-CrN	1.2×10^{-7}	Not hermetic	-
GA-TGI-D6	RP-CrN	$<1 \times 10^{-12}$	Hermetic	Hermetic
N1N3(9)	RP-CrN	$<1 \times 10^{-12}$	Hermetic	Not hermetic
N1N3(10)	RP-Cr	2.9×10^{-10}	Not hermetic	-
GA-TGI-D2	RP-Cr	$<1 \times 10^{-12}$	Hermetic	Hermetic
N1N3(13)	TM-TiN	$<1 \times 10^{-12}$	Hermetic	Not hermetic
GA-TGI-D3	TM-TiN	$<1 \times 10^{-12}$	Hermetic	Hermetic

Five out of eight samples showed extremely low helium leakage rates, indicating gas tightness in atmosphere. The TM-TiN and RP-CrN coated samples were all hermetic, whereas one RP-Cr coated sample was hermetic and the other was not. The TM-CrN coated samples were not impressive with respect to gas tightness based on this initial evaluation. However, because the fraction of helium in the air was only 5.2 ppm, it is unknown whether these five “hermetic” coated samples would still be hermetic in a pressurized gas environment. Of course, it is apparent that GA-TGI-D7, N1N3(7), and N1N3(10) will not have gas tightness in pressurized gas environments because large helium leakage rates were observed when they were exposed in air at atmosphere pressure.

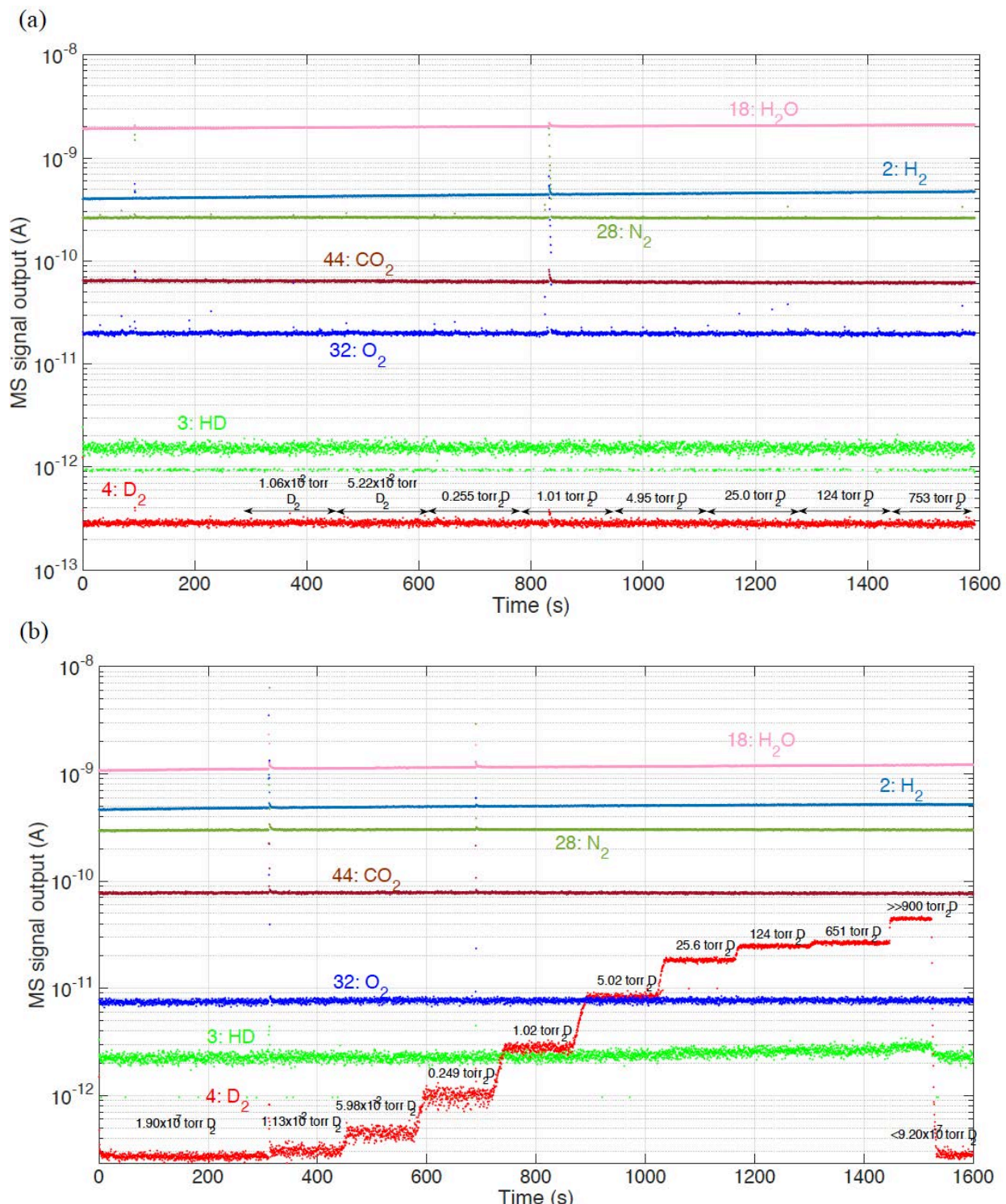
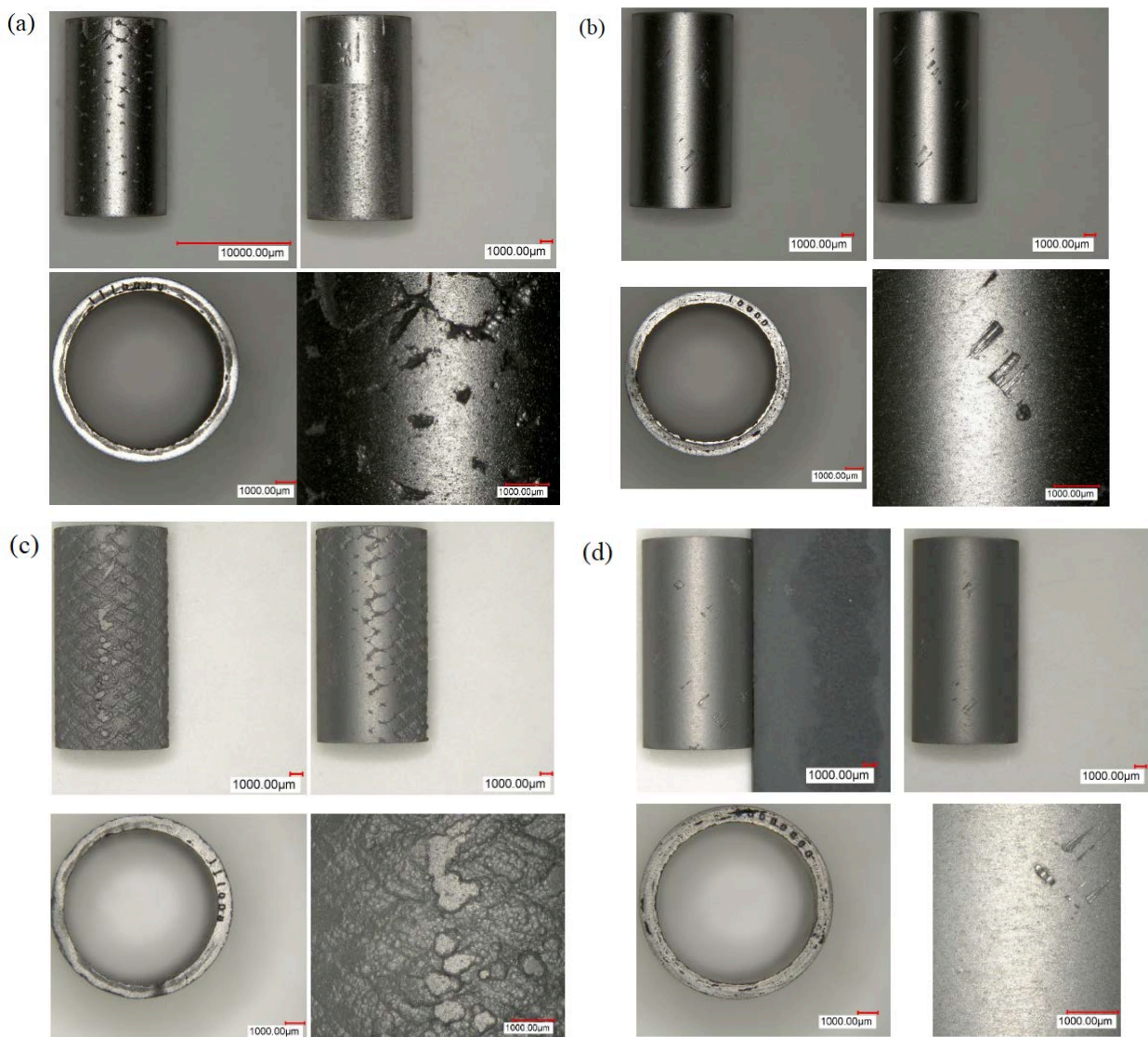


Figure 11. Mass spectrometer signals of gas elements captured in the downstream section of the permeation testing station of coated (a) GA-TGI-D6 and (b) N1N3(9) samples as a function of deuterium pressure. The major remaining gas elements in the system are also shown.

The five “hermetic” samples were further tested in pressurized helium and deuterium environments by measuring the gas permeation flux through the tubular samples using the quadrupole mass spectrometer in the permeation testing system. The testing results indicated that GA-TGI-D6, GA-TGI-D2, and GA-TGI-D3 coated samples were hermetic in pure helium and deuterium environments at pressures up to 1.2 bar, manifested by the extremely low gas leakage rate. In contrast, obvious gas leaking was observed in N1N3(9) and N1N3(13) in pressurized gas environments.

Figure 11a and 11b shows the typical measurement data for a hermetic sample (GA-TGI-D6) and a non-hermetic sample (N1N3(9)), respectively. Complete testing results can be found in the Appendix A. The permeation testing of coated SiC/SiC composite tubes indicated that even the samples using the same coating method performed differently.



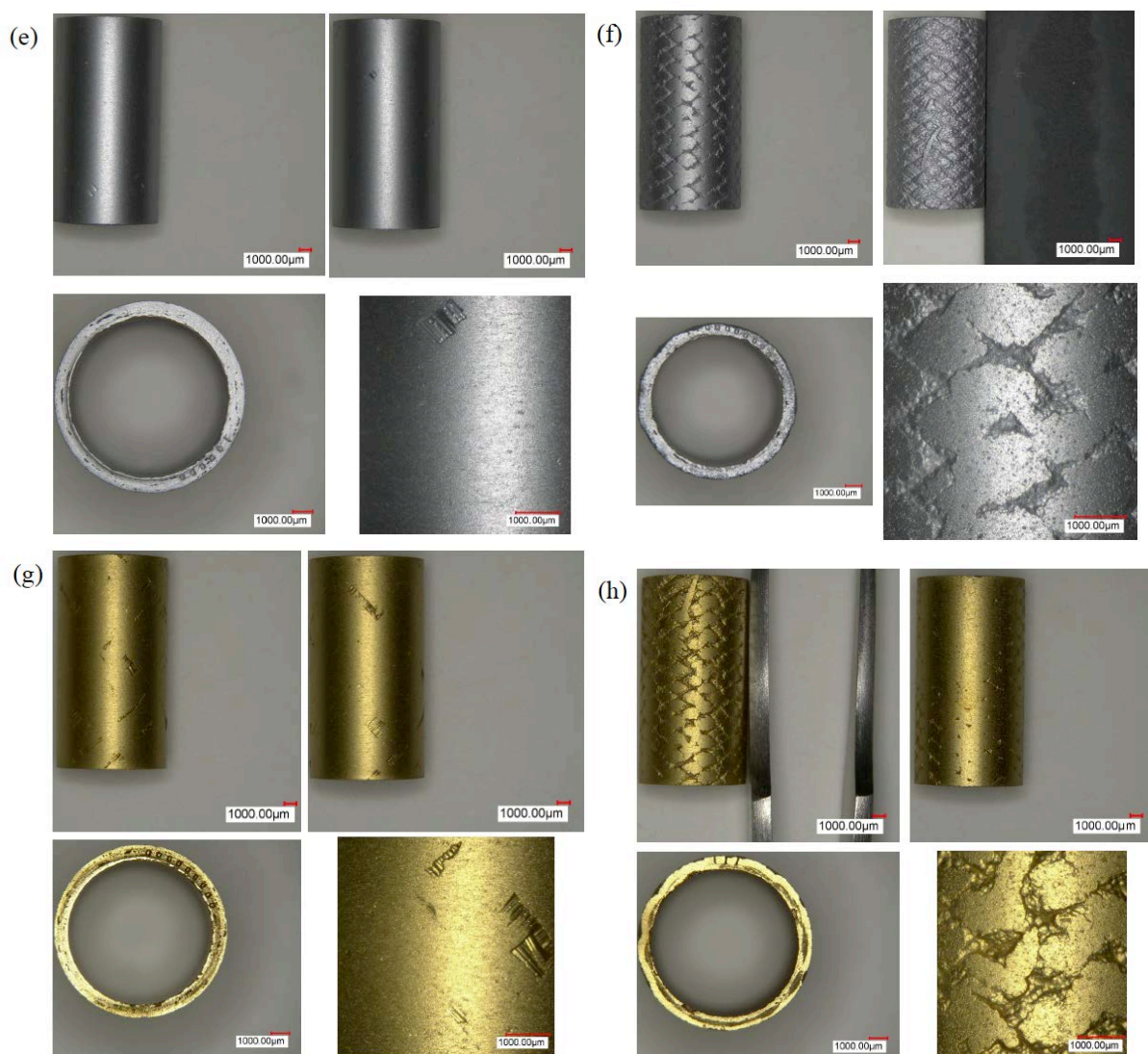


Figure 12. Images of coated (a) GA-TGI-D7, (b) N1N3(7), (c) GA-TGI-D6, (d) N1N3(9), (e) N1N3(10), (f) GA-TGI-D2, (g) N1N3(13), and (h) GA-TGI-D3.

Figure 12 shows the images of the eight tested samples. The two samples coated with TM-CrN have obvious defected areas on the surfaces (Figure 12a and 12b), which might lead to a loss of gas tightness during the testing. Although coated GA-TGI-D6, GA-TGI-D2 and GA-TGI-D3 showed a clear architecture of the bundles (Figure 12c, f, and h), they are still hermetic, implying that the coating materials fully fill in the openings in the sample surfaces and have better adhesion to the SiC/SiC composite samples. N1N3(9) and N1N3(13) (Figure 12d and g), did not retain their gas tightness in a pressurized gas environment. The local defected areas might have been vulnerable to a loss of hermeticity. In addition, these two samples had a better sample surface finishing, implying that more damage (penetrating cracking) likely occurred during the additional surface treatments. More effort is needed to improve the coating qualities to provide consistent performance with respect to gas tightness.

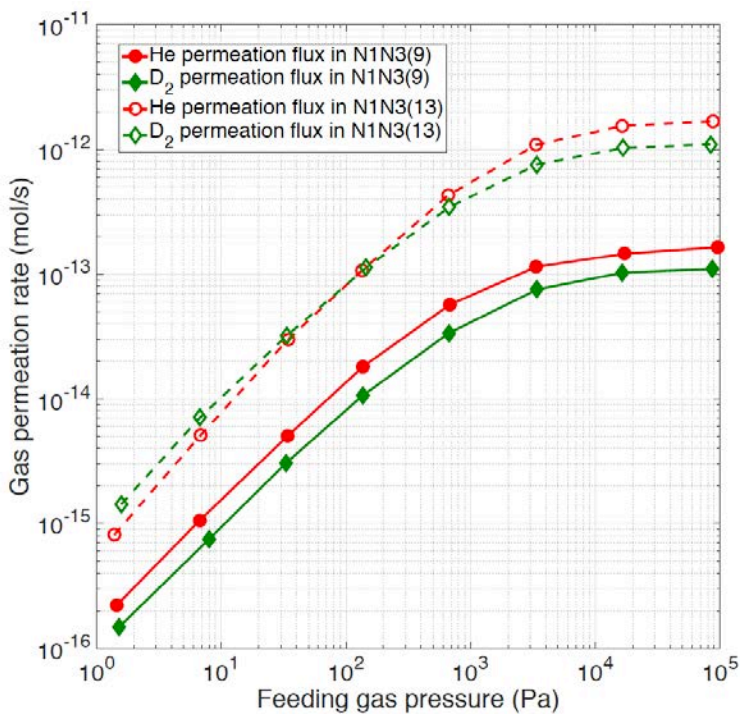


Figure 13. Helium and deuterium permeation flux through the coated N1N3(9) and N1N3(13) tubes as a function of feeding gas pressure.

Figure 13 shows a comparison of the correlations between the permeation flux and feeding gas pressure for N1N3(9) and N1N3(13). Generally, the gas permeation behavior is quite similar to that of a bare SiC/SiC composite tube, N3(10), shown in Figure 10. As the applied gas pressure increased in the pressure range from 10⁻² to 900 torr, the measured gas permeation flux increased and finally approached saturation. It is unclear whether the saturation persisted as the pressure increased further.

Figure 13 shows the deuterium permeation flux in N1N3(13) exceeded the helium permeation flux when the feeding gas pressure was lower than 5 torr. This could be rationalized by the fact that pressurized helium testing was carried out first; and the final high pressure (900 torr) might have induced more cracking inside the wall, leading to the larger permeation flux in the subsequent pressurized deuterium testing. When the helium pressure was greater than 125 torr, the helium permeation flux started to exceed the deuterium permeation flux, showing the same behavior as N1N3(9), which was attributed to the high mobility of helium. The overall larger helium and deuterium permeation flux through N1N3(13) implied that more penetrating cracking occurred in the sample in comparison with N1N3(9). It is apparent that the gas permeation behavior in these two different samples presented two completely different behaviors, implying that the micro-cracking in these two SiC/SiC composite tubes were different.

The nonlinear correlation between the applied feeding gas pressure and the measured gas permeation flux shown in Figure 13 also imposes challenges to the extrapolation method employed by Gutierrez et al. [14] to compute the maximum allowable helium leakage rate for lab-scale

tubular samples. More effort is needed to establish an accurate correlation between the applied gas pressure and the resultant gas permeation flux through tubular samples.

The coated samples following hermeticity testing are being assembled for neutron irradiation in the High Flux Isotope Reactor (HFIR). The gas tightness testing of these samples with the first-generation dual-purpose coating following neutron irradiation is planned.

3.4 Hermeticity Evaluation of Neutron-Irradiated CVD SiC Tubes Under High Heat Flux From Internal Surface to External Surface

3.4.1 Neutron Irradiation of CVD SiC Under High Heat Flux

The application of SiC-based nuclear fuel cladding in LWRs requires that the structure maintains its hermeticity as it withstands the evolving stress state over the fuel lifetime when exposed to intense neutron irradiation under a prototypic high heat flux (and thus a large temperature gradient across the cladding wall) as the fuel rod internal pressure increases due to a buildup of released fission gas. The high heat flux across the thickness of the cladding in LWR applications ($\sim 0.5\text{--}1 \text{ MW/m}^2$) results in a large temperature gradient in the SiC/SiC cladding due to the low thermal conductivity of this composite that further degrades with radiation damage [21]. The higher radial temperature gradient results in an important stress driver that dominates the strain profile across the cladding thickness—the differential swelling strain across the thickness of the cladding [22]. A special irradiation vehicle was designed and fabricated to test SiC-based cladding under conditions representative of a LWR in order to validate thermal-mechanical models of stress states in the studied materials due to irradiation swelling and differential thermal expansion. The design allows for a constant tube outer surface temperature in the range of $300\text{--}350^\circ\text{C}$ under a representative high heat flux ($\sim 0.66 \text{ MW/m}^2$) during one cycle of irradiation in HFIR (equivalent to 2 dpa). More details regarding the design of this irradiation capsule can be found in Ref. [21]. The results for the irradiated monolithic CVD SiC tube are discussed in the following sections.

3.4.2 Brief Introduction of Post-Irradiation Examination and Modeling of Neutron-Irradiated CVD SiC Tube

Because matrix cracking is inherently a statistical phenomenon, a probabilistic assessment approach involving a model-based thermomechanical analysis together with property evaluation methods is required. After irradiation, multiple characterization experiments were performed on the irradiated CVD SiC samples, including optical microscopy observation, resonant ultrasound spectroscopy (RUS), and Raman spectroscopy.

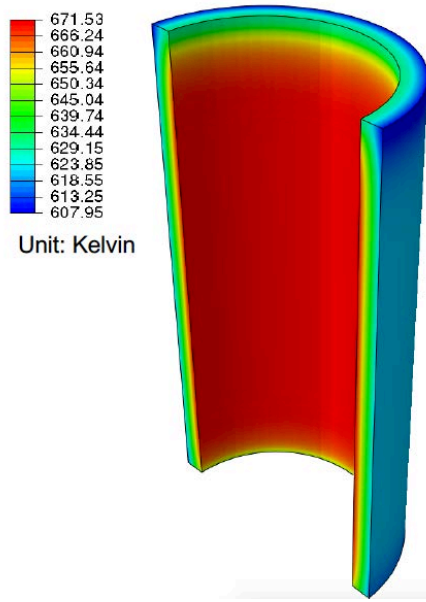


Figure 14. Temperature distribution across the CVD SiC tube during irradiation under a radial high heat flux.

The commercial finite element software Abaqus [23] was used to simulate the temperature distribution across the CVD SiC tube. Figure 14 shows the computed temperature distribution in the CVD SiC sample. The simulated temperatures ranged from 348°C (outside surface) to 399°C (internal surface), with a temperature difference of 51°C. To validate the simulation results, Raman spectroscopy measurements were conducted to acquire the temperature of the studied material during irradiation. The working principle can be found in Ref. [24]. Briefly, neutron irradiation caused a peak shift and broadening of the transverse and longitudinal optical phonon lines. Figure 15a shows the scanning area on the cross section of the neutron-irradiated CVD SiC tube, and Figure 15b presents the correlation between the shift of the longitudinal optical phonon line and the irradiation temperature. The results indicate that the average irradiation temperatures were 332 and 406°C for the two different CVD SiC tubes. This result is reasonable based on the designed average temperature within the CVD SiC tube [21].

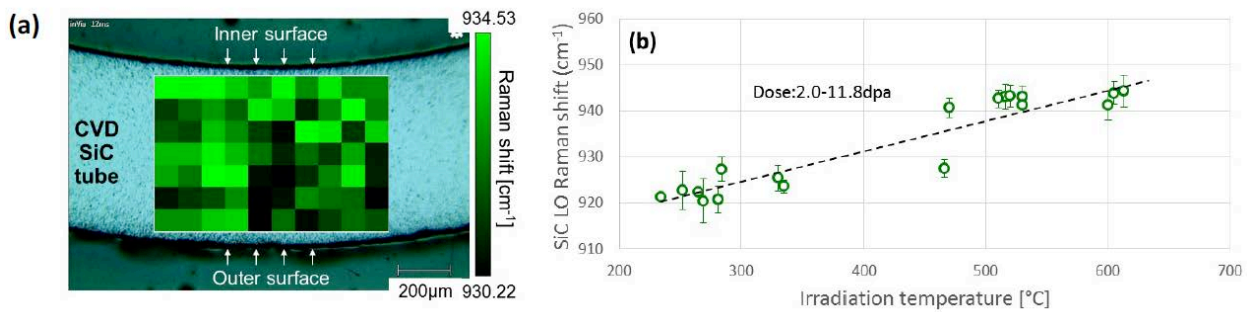


Figure 15. (a) Scanning areas during the Raman spectroscopy measurements; (b) Correlation between the longitudinal optical phonon line shift and the irradiation temperature.

Finite element analysis (FEA) of the neutron-irradiated CVD SiC was performed to predict the stress state at room temperature. The details about this modeling can be found in Ref. [25]. The results are shown in Figure 16. The FEA results show residual tensile axial and hoop stresses of ~ 200 MPa at the inner surface following irradiation, indicating a large probability of cracking in the areas close to the inner surface. On the other hand, the cracking near the outer surface of the cladding is less likely because of the compression stress state along both the axial and circumferential directions.

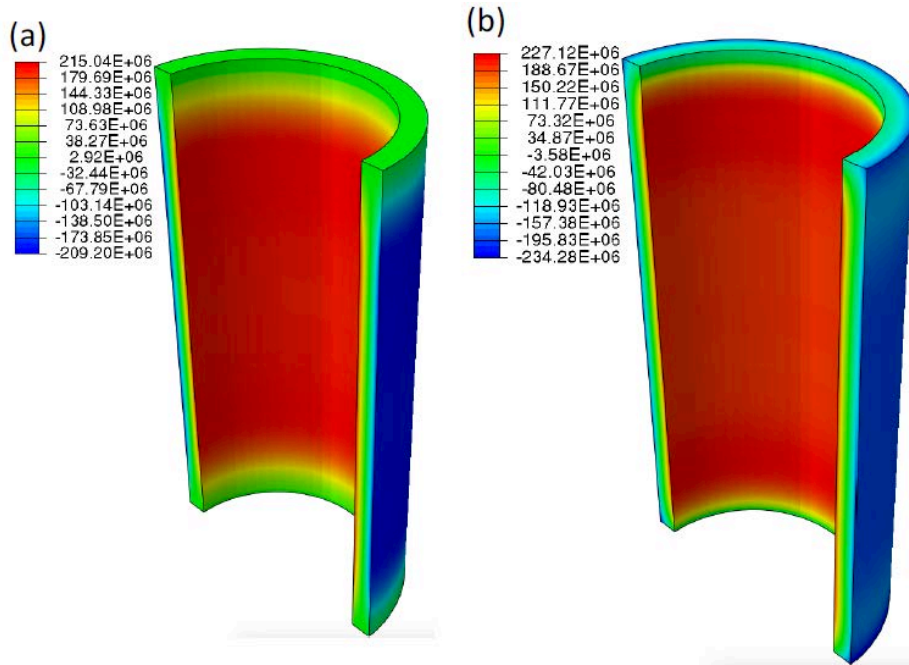


Figure 16. (a) Axial stress and (b) hoop stress distribution in the neutron-irradiated CVD SiC tube. Positive stress indicated tension and negative stress indicates compression (Unit: Pa).

A nondestructive technique, RUS, was used here to evaluate the elastic modulus of the irradiated tubular SiC sample. The details of this technique can be found in the report *M3FT-16OR020202114 – Technique development for modulus, microcracking, hermeticity, and coating evaluation capability for characterization of SiC/SiC tubes* [26]. The frequency spectra for unirradiated and irradiated CVD SiC tube were recorded, as shown in Figure 17. The spectrum shifted leftward following neutron irradiation, implying a change in the elastic modulus induced by the lattice expansion and/or microcracking, both of which are a result from the accumulation of irradiation damages.

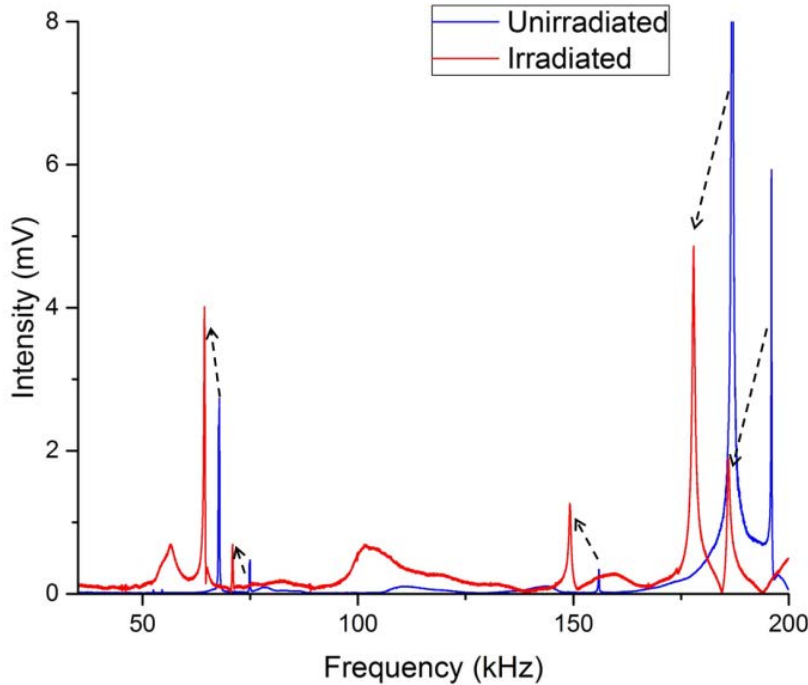


Figure 17. Frequency spectra of unirradiated and irradiated CVD SiC tubes.

The commercial software Insight [27] for automate design exploration and optimization was employed along with Abaqus FEA for iterating the trial elastic properties, namely elastic modulus and Poisson's ratio, and computing the resonance frequencies of the SiC tubes for each set of the elastic properties. The trial sets of elastic modulus and Poisson's ratio that gave the best fit with the RUS measured frequencies were determined for each tube specimen. Figure 18 shows examples of the different vibration modes for an un-irradiated CVD SiC sample. The coordination of modeling and experiment yielded the modulus of the studied specimen. Table 4 lists the results for two neutron-irradiated CVD SiC tubes.

Table 4. Elastic modulus changes for two CVD SiC tubes before and after neutron irradiation.

Elastic Modulus (GPa)	CVD_T1	CVD_T7
As-recieved	444.7	442.2
Neutron-irradiated	399.7	400.8
Difference	-10.1%	-9.4%

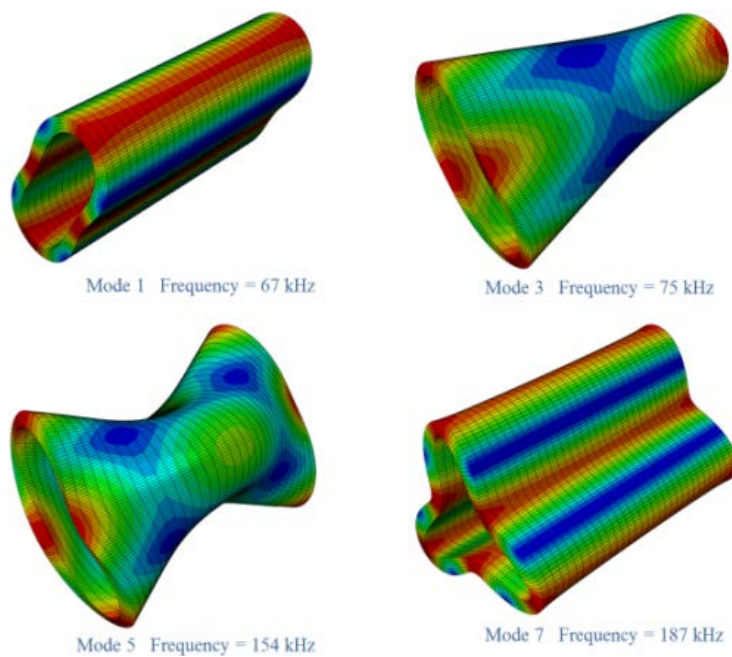


Figure 18. Numerically obtained vibration modes for a CVD SiC tube sample.

Comparing the results with the literature data, it was found that the change in the modulus as a function of swelling for the neutron-irradiated tubular specimen was not consistent with the previous results obtained from the planar CVD SiC samples irradiated without a high heat flux (Figure 19). The difference might be attributed to the existence of micro-cracking in the tubular specimen induced by the residual tensile stress at the inner surface of the sample, which resulted from the large temperature gradient across the sample thickness during the irradiation in this study.

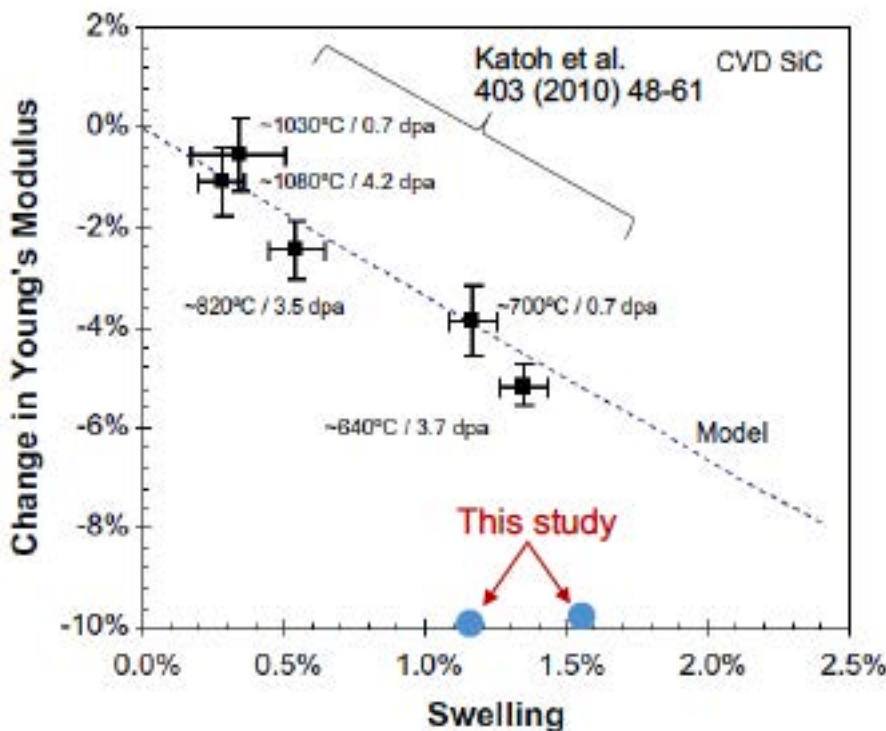


Figure 19. Modulus change as a function of swelling for the neutron-irradiated CVD SiC specimen.

To observe the possible cracking across the specimen, one neutron-irradiated tubular sample and one un-irradiated sample were mounted to epoxy and then cut by using a low-speed diamond saw. Figure 20 shows the cross-section observation of the monolithic CVD tube samples at different selected areas. It is obvious that cracking was observed in the irradiated samples, initiating from the inner surface, consistent with the FEA simulation results that showed significant tensile stress at the inner surface of the tubular sample. Penetrating cracking was also observed, implying a loss of gas tightness in this observed sample.

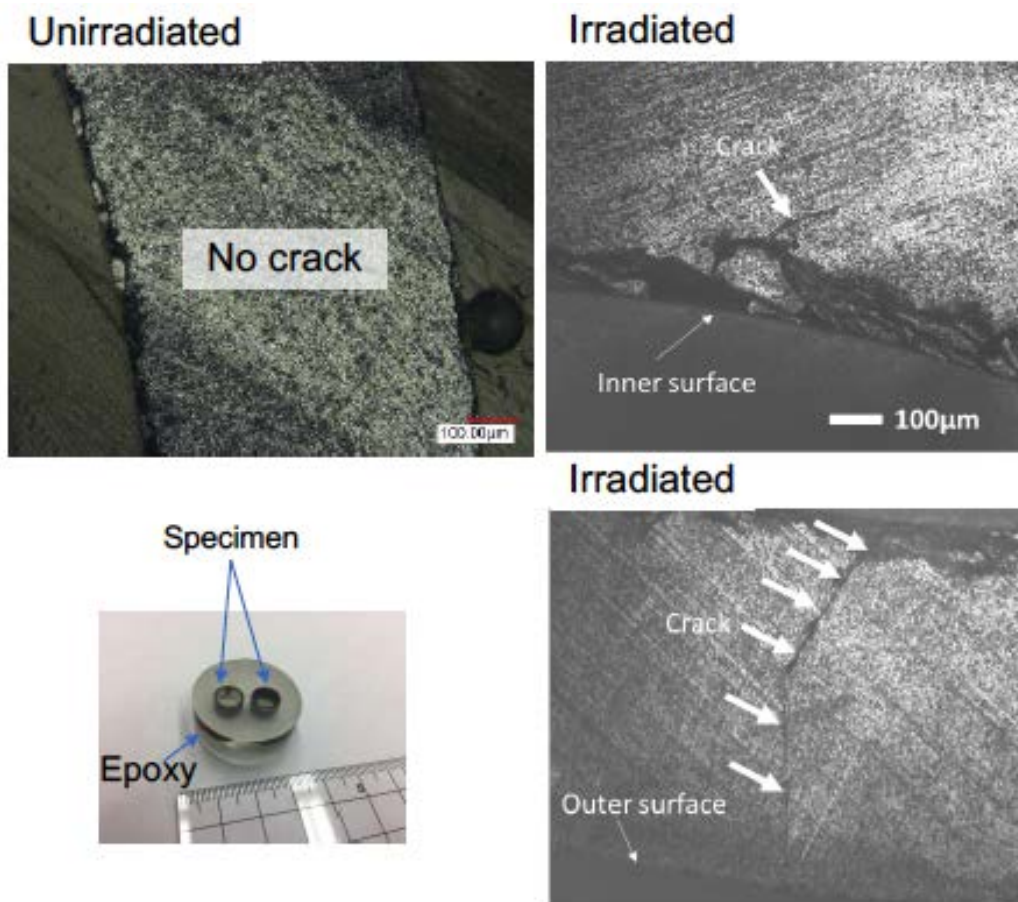


Figure 20. Cross section images of un-irradiated and neutron-irradiated CVD SiC tubular specimens.

3.4.3 Hermeticity Evaluation of Neutron-Irradiated CVD SiC Sample

If penetrating cracking exists in the neutron-irradiated sample, the gas tightness of a CVD SiC tube is expected to fail. The developed permeation testing station is capable of testing the neutron-irradiated samples because the pumping system is a closed loop connected to the ventilation system. Following the same procedure used for testing un-irradiated samples, the helium and deuterium permeation flux through a neutron-irradiated CVD SiC tube was measured. The results are shown in Figure 21, indicating the tested CVD SiC tubular sample following neutron irradiation was still hermetic, as manifested by the extremely low helium and deuterium permeation flux at various gas pressures. Although the RUS measurement, FEA simulation, and optical microscopy observations for other CVD SiC samples irradiated under the same conditions indicated the existence of cracking, the gas tightness of the tested sample was retained, emphasizing the cracking in the CVD SiC is inherently a statistical phenomenon. The hermeticity of the tested sample implies two possibilities: (1) no cracking occurred in the sample or (2) microcracking occurred, but penetrating cracking did not form.

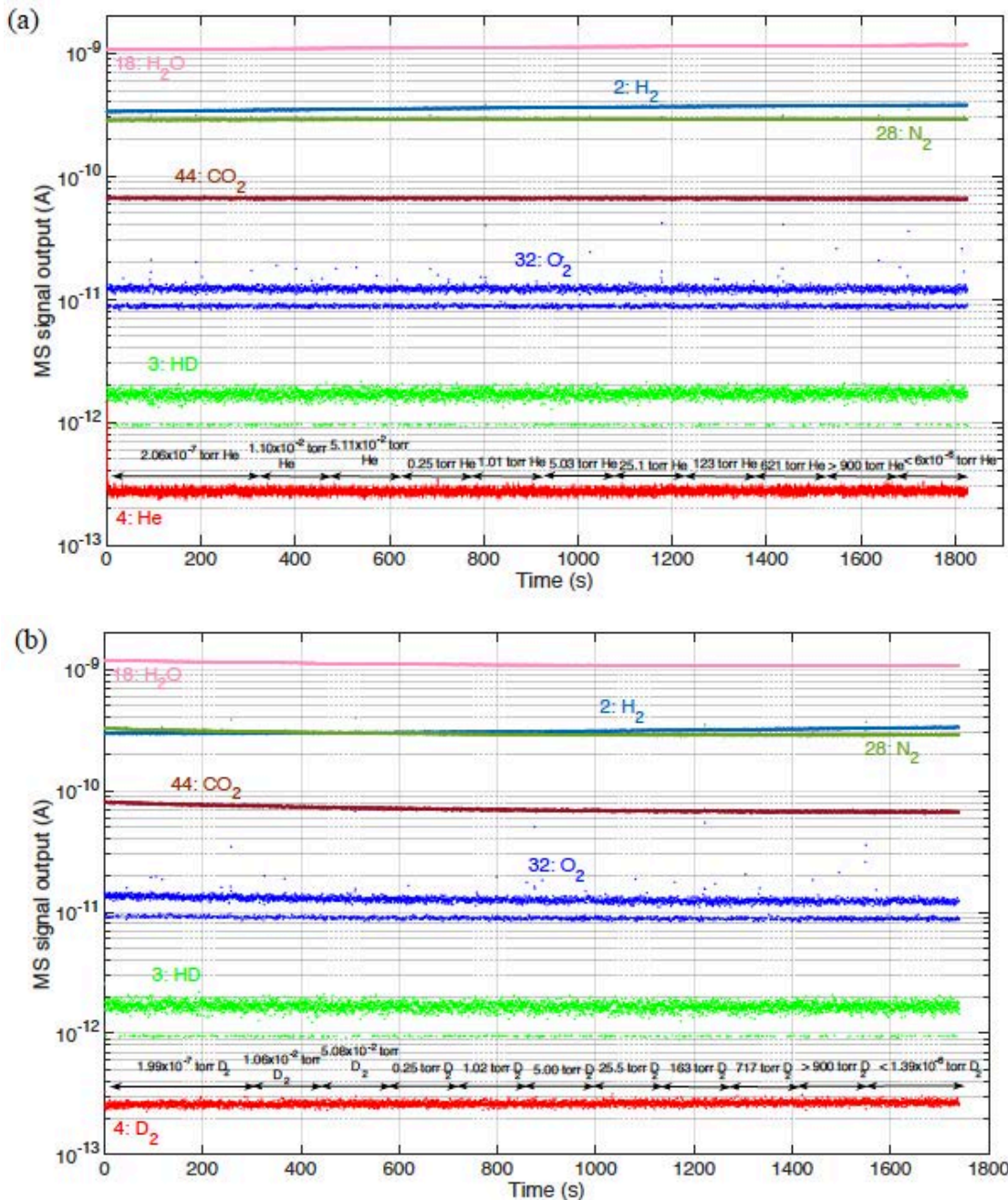


Figure 21. (a) Helium and (b) deuterium permeation flux through neutron-irradiated CVD SiC as a function of applied gas pressure.

4. CONCLUSION AND FUTURE WORK

A comprehensive permeation testing station has been established at ORNL to evaluate the gas tightness of SiC-based nuclear fuel cladding. This report presents details of the design, construction, and calibration of the system, as well as preliminary results for the hermerticity

evaluation of un-irradiated monolithic CVD SiC tubes, uncoated and coated SiC/SiC composite tubes and neutron-irradiated monolithic CVD SiC tubes at room temperature. Crystalbond 590 was used as the primary seal for the tubular samples. The hermetic performance of this sealing medium as well as the ultra-high vacuum enabled the extremely low detection limit of the system at room temperature. The background testing results indicated that this new permeation testing station is capable of measuring helium and deuterium permeation flux through tubular samples as a function of gas pressure at a high resolution of 8.07×10^{-12} atm-cc/s and 2.83×10^{-12} atm-cc/s for helium and deuterium, respectively. The detection limit of this system was sufficient to evaluate the maximum allowable helium leakage rate of lab-scale tubular samples, of which was linearly extrapolated from the evaluation standard used for a commercial as-manufactured LWR fuel rod at room temperature.

The tested un-irradiated monolithic CVD SiC tube was hermetic, as expected, as manifested by an un-detectable deuterium permeation flux at various pressures. A large helium leakage rate was detected for the uncoated SiC/SiC tube exposed to atmosphere, emphasizing the importance of developing coatings with enhanced gas tightness and hydrothermal corrosion resistance. The hermeticity of eight PVD-coated SiC/SiC composite tubes with four types of coating materials was tested. The results showed that the coating performance varied for the different samples. The two SiC/SiC composite tubes coated with TM-CrN were not hermetic. Three SiC/SiC composite tubes provided by General Atomics coated with RP-CrN, RP-Cr, and TM-TiN demonstrated the required gas tightness by showing extremely low gas permeation flux at various applied gas pressures. The other three samples provided by CEA France were not hermetic, although the same coating materials were applied. The results indicated that the hermeticity performance of the coated materials was strongly dependent on the coating materials and the preparation of the substrate SiC/SiC composite samples. More effort is needed to increase the coating quality and ensure the consistent performance of the coated materials.

To simulate the practical application environment in LWRs, monolithic CVD SiC tubes were exposed to neutron irradiation in the HFIR under high heat flux from the internal surface to the external surface. FEA simulation results indicated that the combined neutron irradiation and high heat flux gave rise to a high probability of cracking near the inner surface of the cladding, resulting from the ~200 MPa tensile axial and hoop stresses. RUS measurement confirmed the existence of microcracking within the tubular sample. Optical microscopy observation of the sample cross section found cracks initiating from the inner surface, consistent with the FEA predictions. However, the neutron-irradiated CVD SiC tube tested in the permeation testing station still retained its hermeticity. This result highlights the fact that the micro-cracking in SiC is an inherently statistical phenomenon.

With regard to the future work, the maximum allowable pressure in the upstream chamber of the system is currently limited to 900 torr. Higher pressure capability is required to extract a reliable correlation between the feeding gas and the resultant gas permeation flux. Moreover, it is noted that all experiments conducted in this report were performed at room temperature. A capability of high temperature testing needs to be developed to realize the hermeticity evaluation of SiC-based cladding materials at elevated temperatures.

In summary, the developed permeation testing station is capable of measuring the gas permeation flux in the range of interest with full confidence based on the results discussed. It is considered a

critical pre-/post-irradiation examination technique for characterizing SiC-based cladding materials in as-received and irradiated states to aid the research and development of ATFs.

5. ACKNOWLEDGEMENT

The authors would like to thank Christian M. Petrie and Caen K. Ang for technical review of the manuscript, and Charles Ross Schaich and James Kiggans for their technical supports during the design and construction of the system. The authors are grateful for the support from the staff in the Low Activation Materials Development and Analysis laboratory. Neutron irradiation and the post-irradiation examination of CVD SiC samples were partially supported by the Nuclear Science User Facility. The presented research in this report was sponsored by the Advanced Fuels Campaign of the Fuel Cycle R&D program, Office of Nuclear Energy, US Department of Energy, under contact DE-AC05-00OR22725 with UT-Battelle, LLC.

6. REFERENCES

- [1] S. J. Zinkle, K. A. Terrani, J. C. Gehin, L. J. Ott, and L. L. Snead, Journal of Nuclear Materials **448**, 374 (2014).
- [2] S. J. Zinkle, K. A. Terrani, and L. L. Snead, Current Opinion in Solid State and Materials Science **20**, 401 (2016).
- [3] K. A. Terrani, S. J. Zinkle, and L. L. Snead, Journal of Nuclear Materials **448**, 420 (2014).
- [4] B. A. Pint, K. A. Terrani, M. P. Brady, T. Cheng, and J. R. Keiser, Journal of Nuclear Materials **440**, 420 (2013).
- [5] C. J. Rosa, Journal of the Less Common Metals **16**, 173 (1968).
- [6] Y. Katoh and K. A. Terrani, ORNL/TM-2015/454 (2015).
- [7] L. L. Snead, T. Nozawa, Y. Katoh, T.-S. Byun, S. Kondo, and D. A. Petti, Journal of Nuclear Materials **371**, 329 (2007).
- [8] R. J. Price, Nuclear Technology **35**, 320 (1977).
- [9] A. Hasegawa, A. Kohyama, R. H. Jones, L. L. Snead, B. Riccardi, and P. Fenici, Journal of Nuclear Materials **283-287**, 128 (2000).
- [10] Y. Katoh, K. Ozawa, C. Shih, T. Nozawa, R. J. Shinavski, A. Hasegawa, and L. L. Snead, Journal of Nuclear Materials **448**, 448 (2014).
- [11] M. Ben-Belgacem, V. Richet, K. A. Terrani, Y. Katoh, and L. L. Snead, Journal of Nuclear Materials **447**, 125 (2014).
- [12] K. A. Terrani, Y. Yang, Y. J. Kim, R. Rebak, H. M. Meyer, and T. J. Gerczak, Journal of Nuclear Materials **465**, 488 (2015).
- [13] C. P. Deck, G. M. Jacobsen, J. Sheeder, O. Gutierrez, J. Zhang, J. Stone, H. E. Khalifa, and C. A. Back, Journal of Nuclear Materials **466**, 667 (2015).
- [14] O. Gutierrez, H. E. Khalifa, C. P. Deck, C. A. Back, and R. Schleicher, Transactions of the American Nuclear Society **110**, 803 (2014).
- [15] R. A. Causey, W. R. Wampler, J. R. Retelle, and J. L. Kaae, Journal of Nuclear Materials **203**, 196 (1993).
- [16] R. A. Causey, J. D. Fowler, C. Ravanbakht, T. S. Elleman, and K. Verghese, Journal of The American Ceramic Society **61**, 221 (1978).

- [17] T. Hino, E. Hayashishita, Y. Yamauchi, M. Hashiba, Y. Hirohata, and A. Kohyama, *Fusion Engineering and Design* **73**, 51 (2005).
- [18] T. Hino, E. Hayashishita, A. Kohyama, Y. Yamauchi, and Y. Hirohata, *Journal of Nuclear Materials* **367-370**, 736 (2007).
- [19] H. E. Khalifa, C. P. Deck, O. Gutierrez, G. M. Jacobsen, and C. A. Back, *Journal of Nuclear Materials* **457**, 227 (2015).
- [20] C. K. Ang, K. A. Terrani, J. Burns, and Y. Katoh, **ORNL/TM-2016/332** (2016).
- [21] C. M. Petrie, T. Koyanagi, J. L. McDuffee, C. P. Deck, Y. Katoh, and K. A. Terrani, *Journal of Nuclear Materials* **491**, 94 (2017).
- [22] Y. Katoh, L. L. Snead, C. M. Parish, and T. Hinoki, *Journal of Nuclear Materials* **434**, 141 (2013).
- [23] <https://www.3ds.com/products-services/simulia/products/abaqus/latest-release/>.
- [24] T. Koyanagi, M. J. Lance, and Y. Katoh, *Scripta Materialia* **125**, 58 (2016).
- [25] G. Singh, K. A. Terrani, and Y. Katoh, *Journal of Nuclear Materials* (2017), submitted.
- [26] X. Hu, C. K. Ang, G. P. Singh, and Y. Katoh, **ORNL/TM-2016/372** (2016).
- [27] <https://www.3ds.com/fileadmin/PRODUCTS-SERVICES/SIMULIA/RESOURCES/simulia-isight-brochure.pdf>.

Appendix A

Permeation Testing Results For All Five Coated Samples That Are Hermetic In Atmosphere

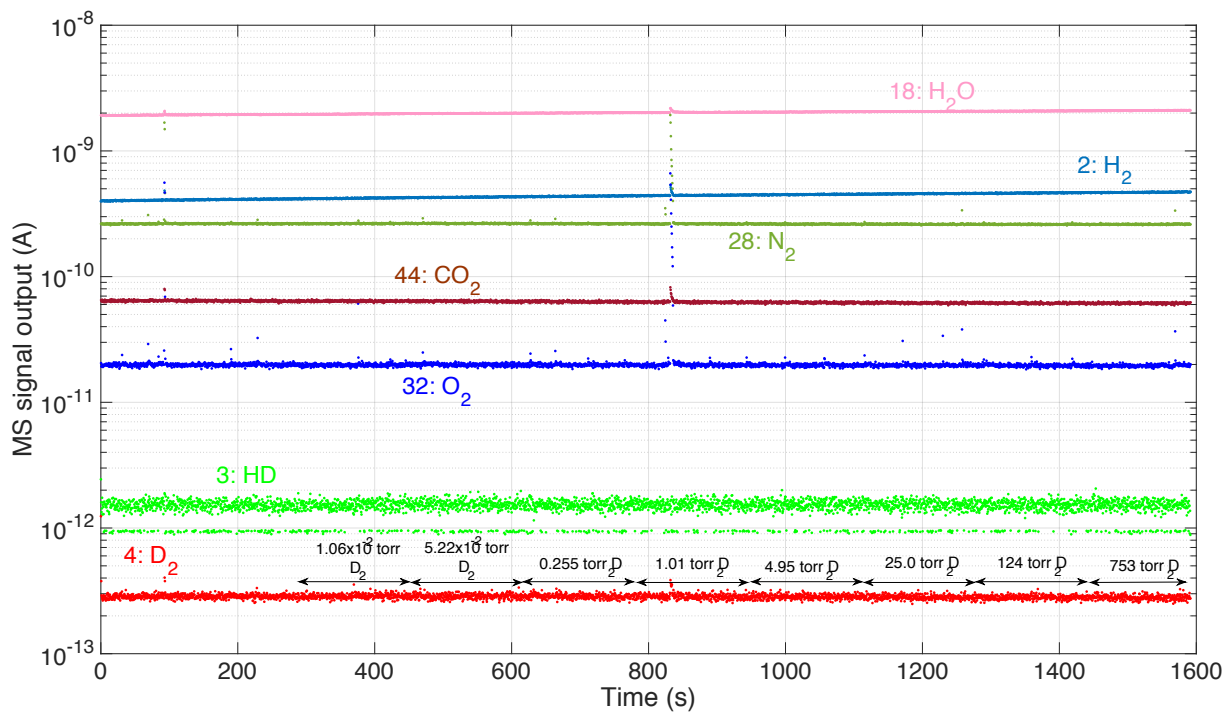


Figure A1. Mass spectrometer signals of gas elements captured in the downstream section of the permeation testing station of coated GA-TGI-D6 as a function of deuterium pressure, indicating its hermeticity in pressurized environment.

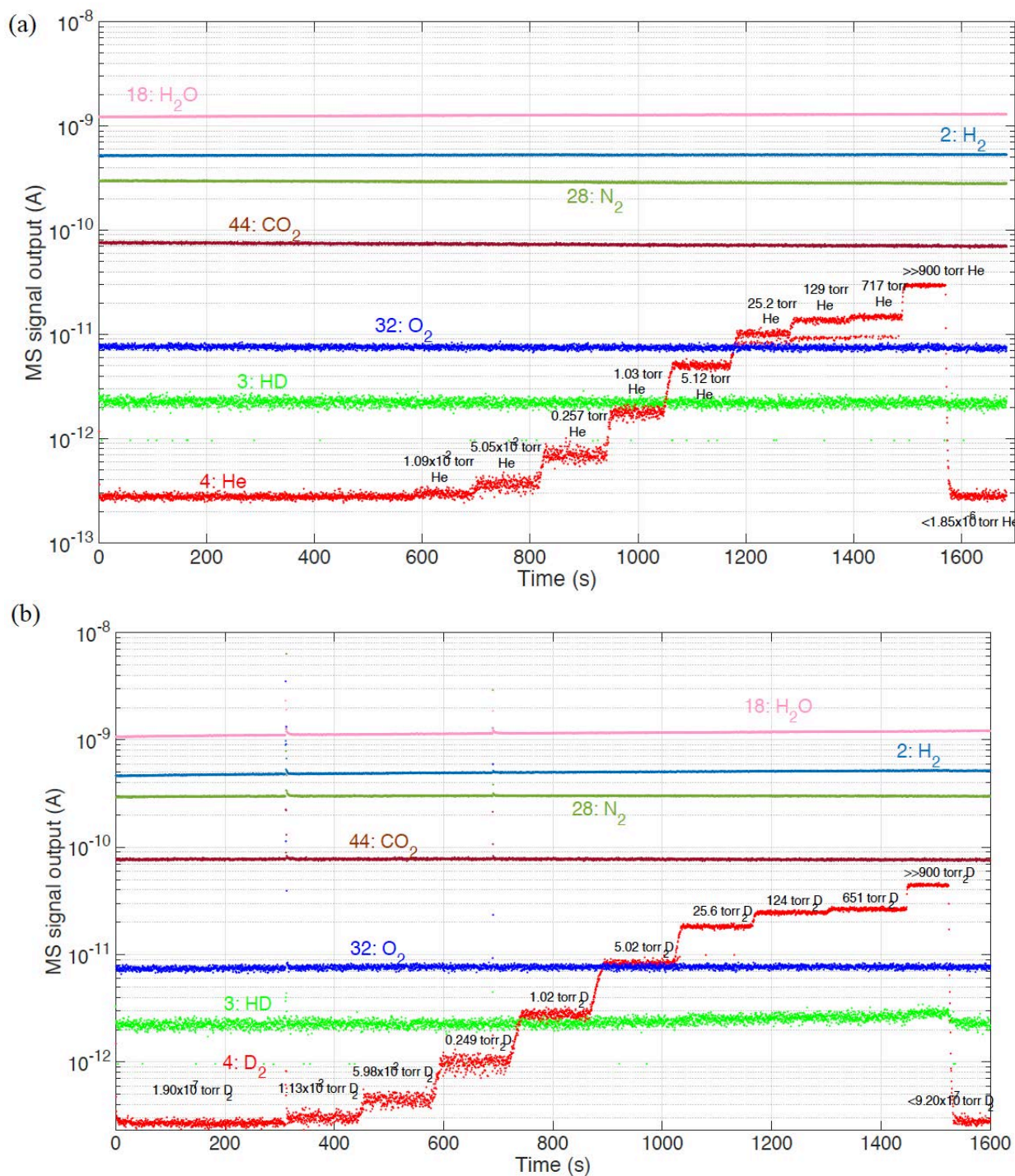


Figure A2. (a) Helium and (b) deuterium permeation flux through N1N3(9) as a function of applied gas pressure. The N1N3(9) is not hermetic in the pressurized gas environment.

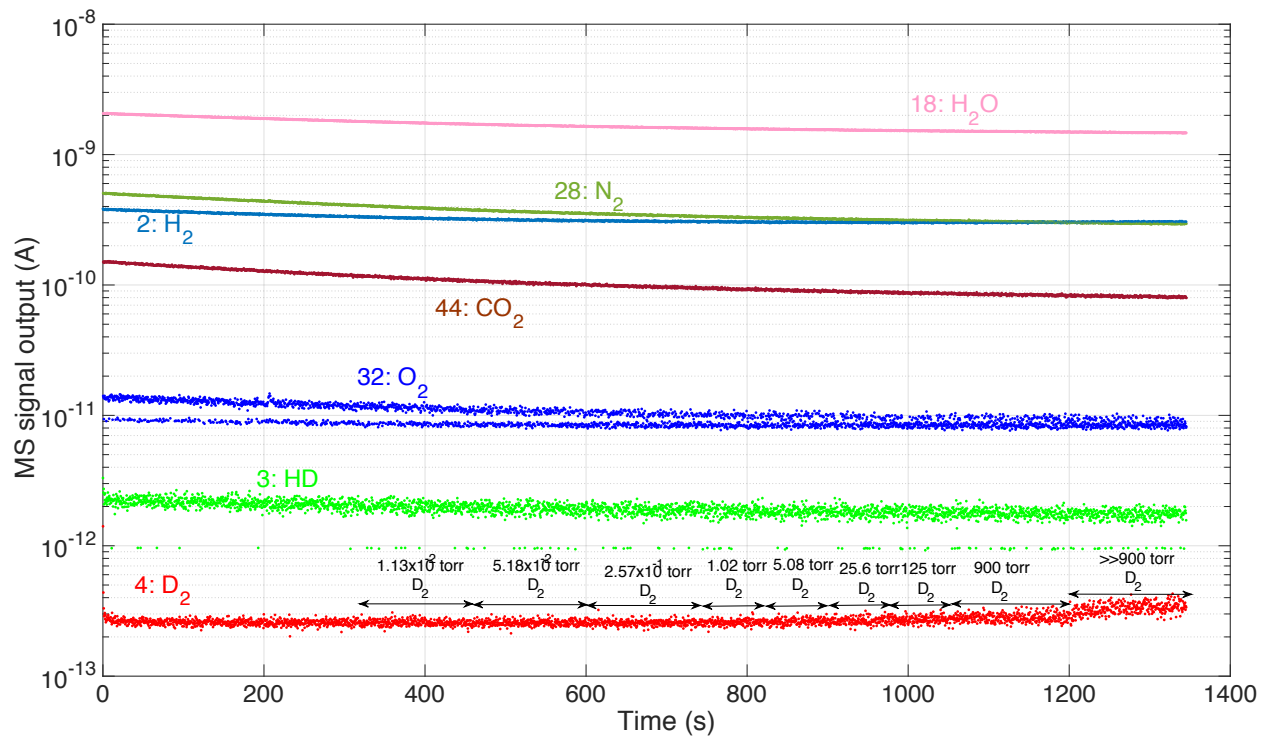


Figure A3. Mass spectrometer signals of gas elements captured in the downstream section of the permeation testing station of coated GA-TGI-D6 as a function of deuterium pressure, indicating its hermeticity in pressurized environment.

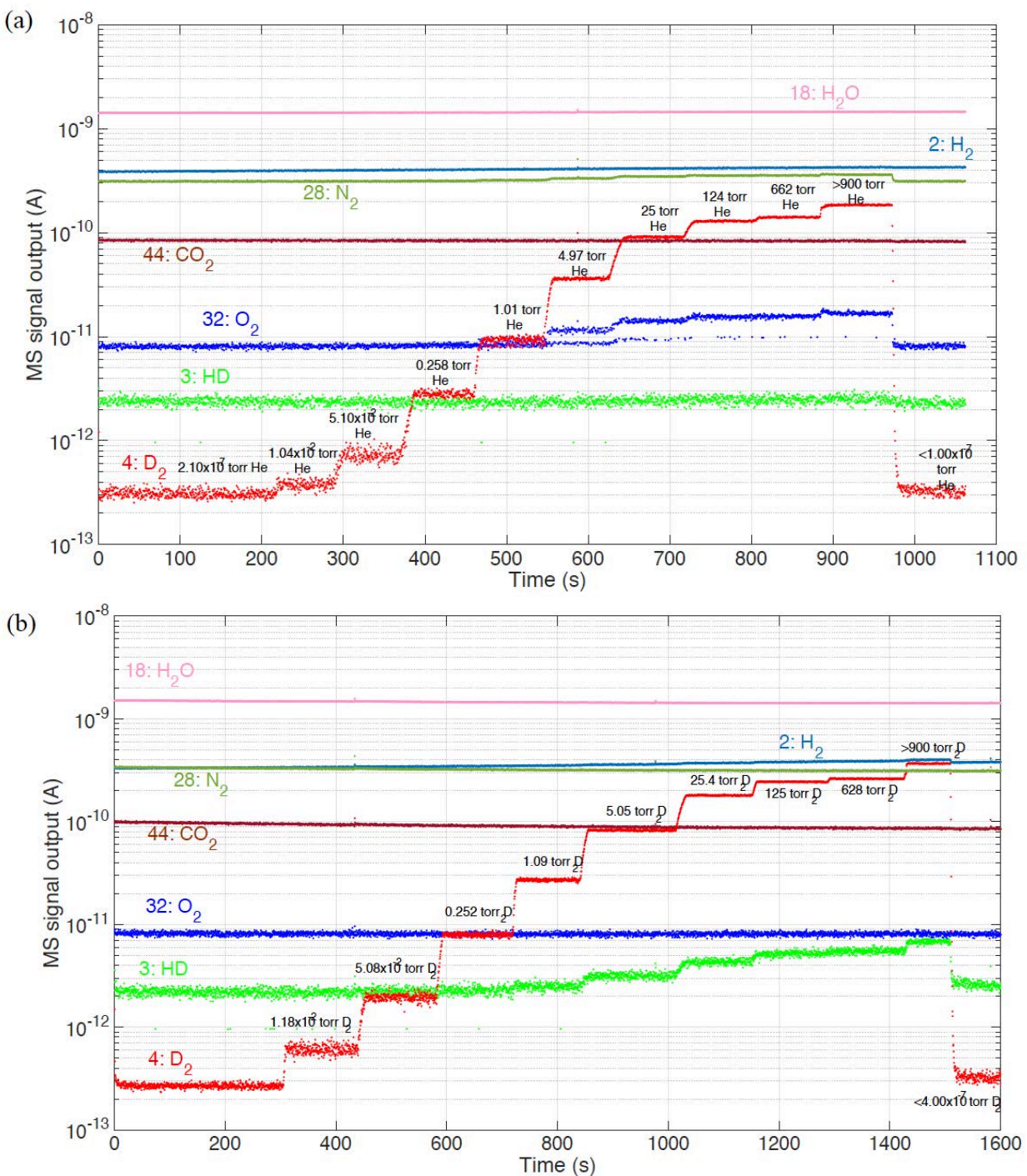


Figure A4. (a) Helium and (b) deuterium permeation flux through N1N3(13) as a function of applied gas pressure. The N1N3(13) is not hermetic in the pressurized gas environment.

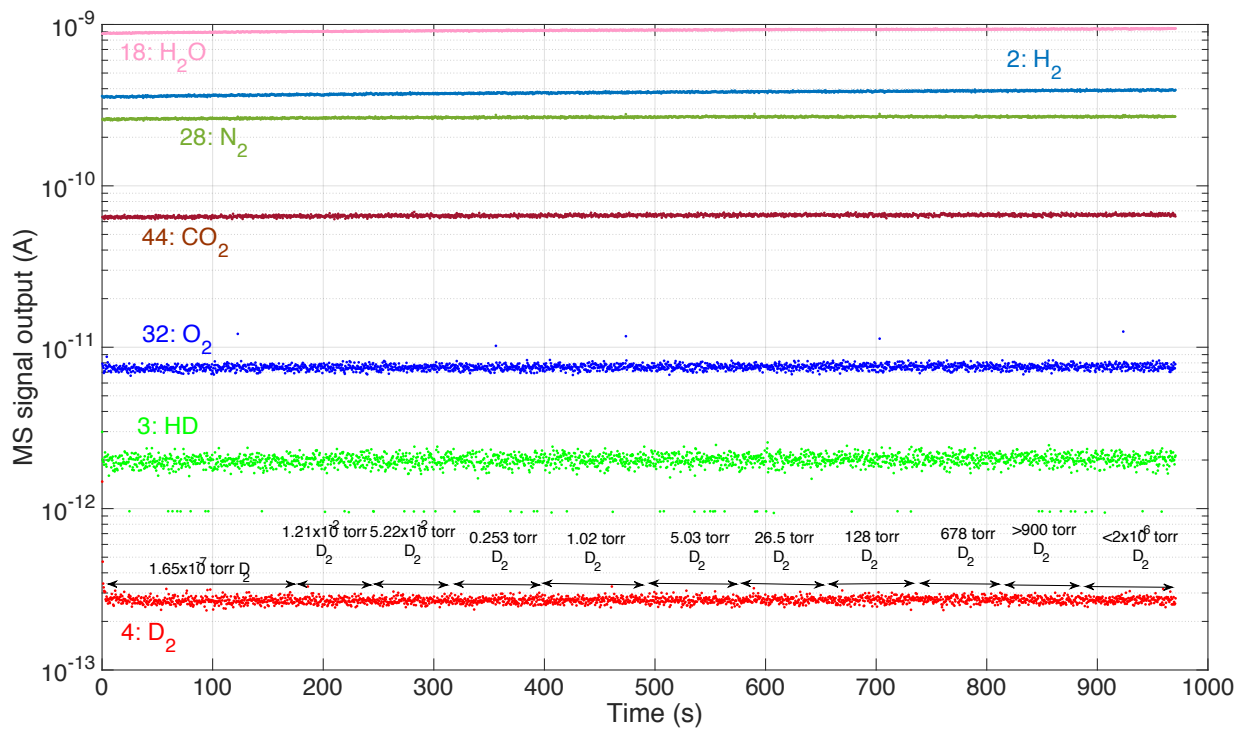


Figure A5. Mass spectrometer signals of gas elements captured in the downstream section of the permeation testing station of coated GA-TGI-D3 as a function of deuterium pressure, indicating its hermeticity in pressurized environment.